Treball Final de Grau
Enginyeria Física

Implementation of a network of nuclear reactions of moderate size aimed at simulating Type Ia supernova explosions.

June 28, 2021

Autor: Axel Sanz

Director: Domingo García Senz

Co-Director: Rubén M. Cabezón

Grau en Enginyeria Física

Escola Tècnica Superior
d'Enginyeria de Telecomunicacions de Barcelona

Universitat Politècnica de Catalunya

Dedicado a:

Mi madre, que me ha aguantado cada día y siempre me preguntaba "oye, cuánto te queda?". Pues ya no me queda nada mama, ya no.

Mis yayos, que sé que les va a hacer muchísima ilusión esto y van a ir presumiendo de esto a todo el mundo.

Los lapones, por darme ánimos cuando me venía abajo.

Ingrid, por ayudarme a hacer el mejor póster del mundo y tener una paciencia increíble.

Ulises, Sandra, Sánchez, Acha i Ker. Por estar ahí, siempre dispuestos a una birra tonta o un musiqueo improvisado.

Karima, Àlex y Aina. Cómo hemos llegado hasta aquí chavales?

Los malardos del Destiny, por hacerme compañía mientras me pasaba el día entero redactando.

Toda mi familia en general, que aunque os veo menos que un Gremlin al agua, siempre os tengo presentes.

Y bueno, sobretodo a mi yaya, que te fuiste justo antes de verme acabar esta etapa.

Contents

1 Abstract

A key ingredient in any numerical study of supernova explosions is the nuclear network routine that is coupled with the hydrodynamic simulation code. When these studies are performed in more than one dimension, the size of the network is severely limited by computational issues. Nevertheless, the characteristic size of these networks has been increasing over the years, from around seven nuclei in pioneering multi-D calculations to roughly fifty at present times. The main goal of this work is to improve, optimize and test a nuclear network of 87 nuclei specially addressed to multidimensional studies of both types of supernova explosions, but with emphasis in thermonuclear Type Ia events.

The nuclear network, Net87, is a natural extension of the old α-network with 14 species, Net14, which was routinely used by the UPC-SciCore collaboration to simulate supernova explosions with good results. Net87 includes reactions for neutrons, protons and alpha particles. One relevant, and original, feature is that electron captures on protons have been incorporated into the network, providing a better track of both, the neutronized species and the gas pressure. A second important feature is that the reactions are implicitly coupled with the temperature, which allows for a more stable approach to the nuclear statistical equilibrium regime and to the freeze-out of the reactions during the expansion.

Here we analyze the performance of the Net87 routine in light of both: the computational overhead of the algorithm and the released nuclear energy and produced yields during the combustion in typical Type Ia Supernova (SN Ia) conditions.

2 Introduction

2.1 Nuclear Networks and Type Ia Supernovae simulations

White Dwarfs (WD) are stable stars formed from the core remnants of main-sequence stars that were not massive enough ($\lesssim 8M_\odot$) to start burning their carbon and oxygen content. They are basically sustained by the pressure exerted by the electrons in the degenerate matter and, without any external energy input, these stars are inevitably doomed to slowly decrease its temperature and freeze, since they are not able to ignite their C+O cores.

The electron-degenerate pressure is fundamentally due to the Pauli exclusion principle, which sets a maximum mass condition for these stars known as the Chandrasekhar mass and takes a value of roughly $1.4M_\odot$ [6]. White dwarfs approaching the Chandrasekhar mass-limit are unstable. Depending on the environmental conditions they could collapse (leading to a Core Collapse, Type II Supernova) or experience a thermonuclear explosion (leading to Type Ia Supernova).

Type Ia supernovae explosions (SN Ia) take place after the collision between two white dwarfs (called double degenerate scenario because both stars are WD), or after a single WD accretes mass from its binary main-sequence or giant-like star companion (single degenerate scenario because only one of the stars is a WD, see figure 1.

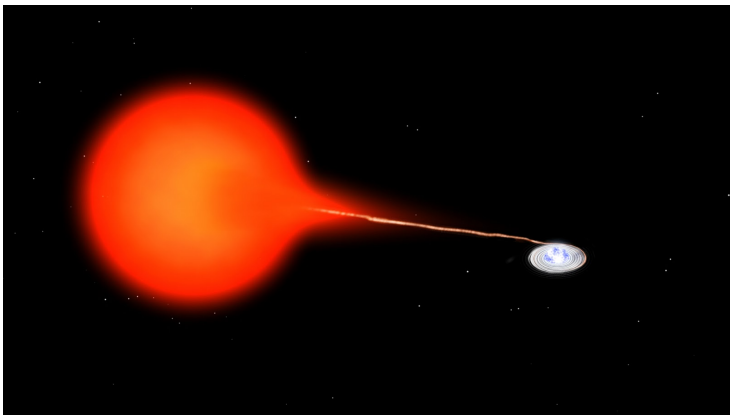

Figure 1: Artistic representation of a White Dwarf accreting mass from its companion. Bill Saxton, NRAO/AUI/NSF

The explosion occurs due to the ignition of either the core of the white dwarf, composed of a mixture of carbon and oxygen, or the helium in the surface layers. The ignition initiates a chain of nuclear reactions producing a great number of new elements and releasing a huge amount of energy from the fusion.

The main product of the nucleosynthesis during SN Ia is the isotope ^{56}Ni which is a radioactive nuclei with a half-life time of roughly 6 days. After the explosion, the expanding material is mainly comprised of this nuclei, which decays to ^{56}Co and then to ^{56}Fe producing high-energy photons. This continued source of photons gives SN Ia explosions a very characteristic luminosity curve with a pronounced peak around $10^{10}L_\odot$ (See figure 2). Moreover, since most SN Ia originate from similar conditions (from near Chandrasekhar-mass WD), the maximum luminosity peak has a very similar value in all SN Ia explosions. These two features of the light curve make SN Ia ideal to measure precise distances, this is why they are used as standard candles.

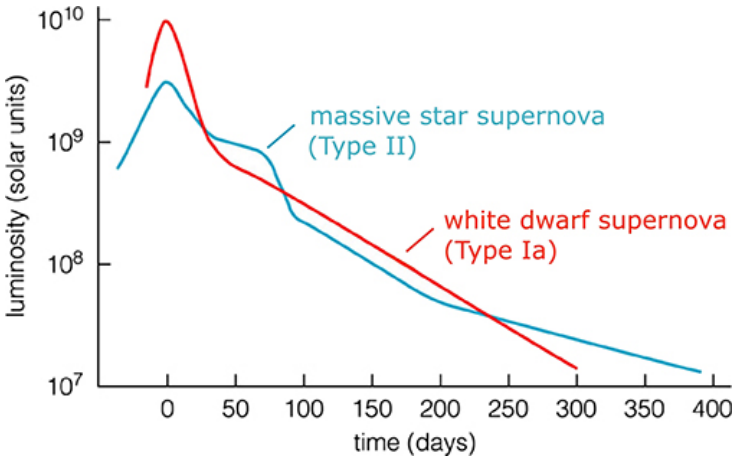

Figure 2: Luminosity evolution of Type Ia and Type II supernova (IOPscience-Institute of Physics)

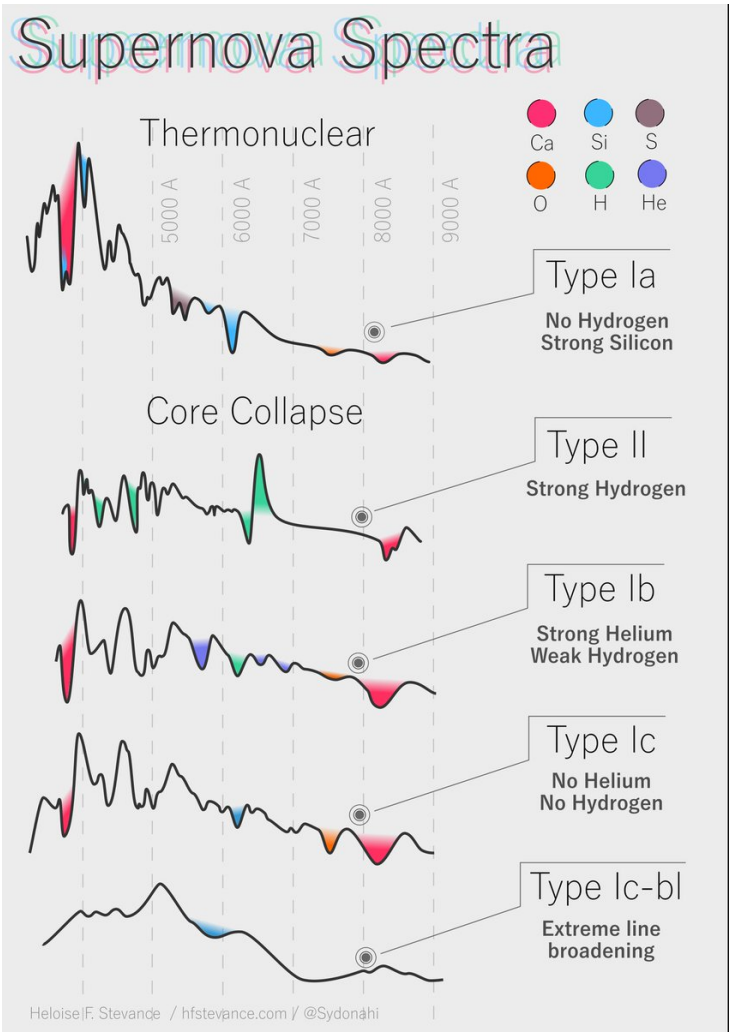

Figure 3: Presence of distinctive lines in the spectra of different supernova types (Daniel Kasen-Supernova spectra page).

As the luminosity decreases over months, the emitted spectra of SN Ia changes its main peaks (i.e. the main elements of the spectra are not constant). This is due to the difference in composition of the inner and outer layers of the star. The outermost layers are composed of the lighter elements and dominate the spectra during the early stages of the expansion. However, once this region expands enough, the material becomes invisible and the inner layers spectra show the dominance of the heavier elements. Figure 3 summarizes the most distinctive spectral features of several supernova types. As we can see, the spectrum of SN Ia does not show hydrogen (as opposite to SN II) but it has strong absorption lines of intermediate-mass elements, especially silicon.

If the WD is close to the Chandrasekhar mass and the accretion of typically hydrogen and helium from the outermost shell of the donor star occurs at certain stable rates, steady H and He burning takes place so that its combustion is gentle and the burnt material is not re-ejected from the surface layers. Thus, the mass of the WD increases and the core is compressed. At some point the carbon is ignited (via the $^{12}C+^{12}C$ reaction) and the subsequent propagation of the combustion through the whole white dwarf provokes its total destruction. In this scenario, called the Chandrasekhar-mass model of SN Ia, the ignition of the core takes place at densities of around 2×10^9 g/cm^3, and combustion is transported by deflagration waves (i.e. subsonically, [11]), detonation waves (i.e. supersonically, [1]) or by a mix of both modes [9].

Another possible outcome is the so called double-detonation scenario. In this case, a sub-Chandrasekhar mass WD accretes material from its donor without reaching the mass limit and accumulates a layer of He without burning it. Eventually, the helium may ignite and detonate (at densities around 10^6 g/cm^3). The detonation blows the tiny He-envelope and sends a strong shock wave towards the $^{12}C+^{16}O$ core. Eventually the carbon fuel ignites provoking a new detonation wave which destroys the whole star [17].

Finally, another scenario relies in the merging of two white dwarfs with single masses of around $0.9M_\odot$. During the process of merging, the carbon fuel may explosively ignite so that the merged object explodes, giving rise to a SN Ia. This is called the Double Degenerate scenario for SN Ia. In this scenario the total mass of the merged object can be larger that the Chandrasekhar-mass limit [12].

Although the first simulations of these events were carried out supposing spherical symmetry, modern studies make use of complex multi-dimensional hydrodynamics. The main aim is to compute the changes in density, temperature, chemical composition and several other magnitudes from first principles (that is minimizing the number of free parameters in the simulations). The topic of this work is indeed one of the subroutines used in these hydrodynamical codes, the nuclear network.

Nuclear networks (or nets) are algorithms used to replicate the nucleosynthesis reactions, such as nuclear fusion or other processes as photo-disintegrations. In the frame of SN Ia, the networks are used to account for the fusion reactions at the carbon and oxygen core, where the ignition of the fuel takes place releasing large amounts of energy and detonating the WD, as well as for the fusion at the outer He-layers on Sub-Chandrasekhar WD. They play a major role in the simulation codes since they are responsible for the creation of new nuclear species and the release or absorption of nuclear energy, leading to the gradients on temperature, pressure, and density that change the thermodynamical properties of the fluid whose dynamics are computed by the rest of the hydrodynamical code.

The poor computation power back in the last quarter of the past century made impossible to carry out multi-dimensional computations in pioneering attempts of simulating explosive supernova events. Moreover, the nuclear networks were seriously limited in the number of species they managed to just 3 or 4 key isotopes. Current SN Ia simulations are performed in two and three dimensions with nuclear networks managing many more different species, from 10-14 isotopes the smaller nets to more than 440 for the largest [13].

2.2 Work Objectives

The main motivation of this work was to complete, improve and optimize an existing nuclear reaction network, Net86, to be used in multi-dimensional hydrodynamic simulations of type Ia Supernovae. Both, this net and its reduced version Net14, were developed back in 2004 by R. M. Cabezón, D. García-Senz, and E. Bravo [4], but only the small net has been actively used coupled with a hydrodynamics code due to its low computational load. Fifteen years after, the computational technology is now much more powerful and the usage of more complex networks is nowadays possible.

The plan of bringing back Net86 required three different steps:

- **The enhancement and optimization of the algorithm.** The goal was to implement an iterative Newton-Raphson solver in order to improve accuracy on the solutions and enlarge the time-steps of integration, as well as extending the integration order to second degree by using semi-implicit discretization of the system of equations.

- **The addition of Electron Capture Reactions.** They are quite important processes in high density combustion and are often dismissed since they need medium to large networks to be implemented in.

- **The testing and analysis of the results.** Once the algorithm is ready, the network needs to be tested in several different scenarios and its results compared to those of Net14, as well as to roughly predict the impact of the new network in upcoming multi-D simulations of SN Ia explosions.

3 The Nuclear Networks

3.1 Mathematical Model

Nuclear networks are described with a set of differential equations, associated with the different species that appear in them, in addition with some extra equations concerning other magnitudes such as entropy, energy or temperature providing stability and robustness to the model. The approach taken in our proposed nets is based on the scheme used by Arnett and Truran [2]. It consists on the equations of the species, solved implicitly, plus an equation for the conservation of energy coupled in explicit manner. Later on, [10] proposed to extend the implicit coupling in the chemical equations to the energy equation. Solving at once the chemical and energy equations with an implicit scheme improves the stability of the integration. However, the price to pay is a more complex algebraic formulation.

According to [4], the equations describing the evolution of the molar fraction Y_i of a general

i-species in a nuclear network are:

$$\frac{dY_i}{dt} = \sum_{k,l} r_{kl} Y_l Y_k - \sum_j r_{ij} Y_i Y_j + \sum_m \lambda_m Y_m - \lambda_i Y_i \tag{1}$$

The terms $r_{ij} = r_{ij}(T) = \rho N_A \langle \sigma, \nu \rangle_{ij}$ correspond to the nuclear reaction rates and $\lambda_i = \lambda_i(T)$ stands for photo-disintegration rates. The discretization of the equations is performed as:

$$\begin{aligned} \frac{Y_i^{n+1} - Y_i^n}{\Delta t} = & \sum_{k,l} r_{kl}(T^{n+\theta}) Y_l^{n+\theta} Y_k^{n+\theta} - \sum_j r_{ij}(T^{n+\theta}) Y_i^{n+\theta} Y_j^{n+\theta} \\ & + \sum_m \lambda_m(T^{n+\theta}) Y_m^{n+\theta} - \lambda_i(T^{n+\theta}) Y_i^{n+\theta} \end{aligned} \tag{2}$$

where the notation $Y_i^{n+\theta} = Y_i^n + \theta \Delta Y_i$ and $T^{n+\theta} = T^n + \theta \Delta T$ is used to determine the degree of implicitness of the system, allowing for explicit, implicit or semi-implicit schemes by varying the value of the parameter θ from 0 to 1. For convenience, a simplified notation $r_{ij}^{n+\theta} \equiv r_{ij}(T^{n+\theta})$ and $\lambda_i^{n+\theta} \equiv \lambda_i(T^{n+\theta})$ is used from now on to avoid charging the expressions. Thus, linearizing the equations:

$$\begin{aligned} \frac{\Delta Y_i}{\Delta t} = & + \theta \sum_{k,l} r_{kl}^{n+\theta} Y_l^{n+\theta} \Delta Y_k + \theta \sum_{k,l} r_{kl}^{n+\theta} Y_k^{n+\theta} \Delta Y_l \\ & - \theta \left(\sum_j r_{ij}^{n+\theta} Y_j^{n+\theta} \right) \Delta Y_i - \theta \sum_j r_{ij}^{n+\theta} Y_i^{n+\theta} \Delta Y_j + \theta \sum_m \lambda_m^{n+\theta} \Delta Y_m - \theta \lambda_i^{n+\theta} \Delta Y_i \\ & + \theta \left(\sum_{k,l} r'_{kl}{}^{n+\theta} Y_l^{n+\theta} Y_k^{n+\theta} - \sum_j r'_{ij}{}^{n+\theta} Y_i^{n+\theta} Y_j^{n+\theta} + \sum_m \lambda'_m{}^{n+\theta} Y_m^{n+\theta} - \lambda'^{n+\theta}_i Y_i^{n+\theta} \right) \Delta T \\ & + \sum_{k,l} r_{kl}^{n+\theta} Y_l^{n+\theta} Y_k^{n+\theta} - \sum_j r_{ij}^{n+\theta} Y_i^{n+\theta} Y_j^{n+\theta} + \sum_m \lambda_m^{n+\theta} Y_m^{n+\theta} - \lambda_i^{n+\theta} Y_i^{n+\theta} \end{aligned} \tag{3}$$

There are N equations, one for each species, but $N + 1$ unknowns since temperature T is also a variable. Hence, an additional equation involving T has to be included in order to solve the system. This equation is the already mentioned energy equation and can be expressed as:

$$dQ = -P \frac{d\rho}{\rho^2} + \frac{\partial U}{\partial \rho} d\rho + \frac{\partial U}{\partial T} dT + \sum_i \left(-BE_i + \frac{\partial U}{\partial Y_i} \right) dY_i \tag{4}$$

where P is pressure, U is the energy per gram of material, BE_i stands for the nuclear binding energy of a mol of the i-species and dQ represent external sources or sinks of energy.

The expression can be simplified using the thermodynamical identity

$$P = T \left(\frac{\partial P}{\partial T} \right)_\rho + \rho^2 \left(\frac{\partial U}{\partial \rho} \right)_T \tag{5}$$

resulting in the new espression:

$$dQ + \sum_i \left(BE_i - \frac{\partial U}{\partial Y_i} \right) dY_i - \frac{\partial U}{\partial T} dT = -T \frac{d\rho}{\rho^2} \left(\frac{\partial P}{\partial T} \right) \tag{6}$$

In general, we will deal with adiabatic processes, so $dQ = 0$. Another important scenario are isochoric combustions, which means $d\rho = 0$ and the energy equation reads as

$$\sum_i \left(BE_i - \frac{\partial U}{\partial Y_i} \right) dY_i - \frac{\partial U}{\partial T} dT = 0 \Rightarrow \sum_i BE_i dY_i = \sum_i \frac{\partial U}{\partial Y_i} dY_i + \frac{\partial U}{\partial T} dT \tag{7}$$

The right hand side of equation 7 is just the change in the internal energy of the gas during an isochoric process. Which is a very intuitive expression since it shows that the energy-loss of the ion gas is stored in the nuclei as binding energies.

Equation 7 can also be discretized the same way as for the species equations, then the linearized system can be solved. This coupling of temperature with the species in the matrix of the system provides stability in NSE regime, as shown by [10], preventing the appearance of oscillations and instabilities when reaching this particular stage of the combustion.

In the energy equation, it is essential to know some magnitudes related to the equation of state (EOS), such as the specific heat of the gas. The implemented EOS [3] consists of a mix of electrons treated as a partially degenerate relativistic gas, an ideal gas of ions, and radiation.

Other interesting features of the network are the possibility to perform isochoric and isothermic processes as well as adiabatic expansions. This expansion is performed by changing the value of density over time as $\rho(t) = \rho_0 e^{-\frac{t-t_0}{t_{hd}}}$, where $t_0 = 5t_{hd}$ is the time the expansion begins and t_{hd} is the characteristic hydrodynamical time of the system. We compute $t_{hd} = 10^{-2}\sqrt{\frac{2\times 10^9}{\rho}}$ for high-density combustions and $t_{hd} = \frac{440}{\sqrt{\rho}}$ for lower densities.

Another feature is the inclusion of coulombic corrections to the rates since at high densities the behaviour of the plasma drifts away from that of an ideal gas of nuclei and electrons. Detailed description of the architecture of the network can be found in [4].

3.2 Net14 and Net86

Figure 4: Scheme of the nuclear reactions network Net14. Red lines represent an alpha-capture, green for triple alpha reaction and yellow and blue for heavy-ion reactions on C and O. Source: https://astro.physik.unibas.ch/net14

Net14 is a small nuclear net working with 14 isotopes, from ^{4}He until ^{60}Zn and is based on alpha captures. It also includes triple alpha and three heavy-ion alpha-producing reactions. It is a very convenient net to compute general behaviour on explosive nucleosynthesis events, since its reduced number of isotopes guarantees low computational cost. According to [16] these reduced networks are able to reproduce the released nuclear energy with at most, 30% error. Nevertheless they only give a very rough idea of the produced yields.

When aiming to implement electron captures, it is necessary to include single protons and neutrons into the network. Nevertheless, the inclusion of both these new species also requires the addition of several new isotopes, including more neutronized species of already-included elements and new odd atomic number elements which were not conceived in the original alpha-chain.

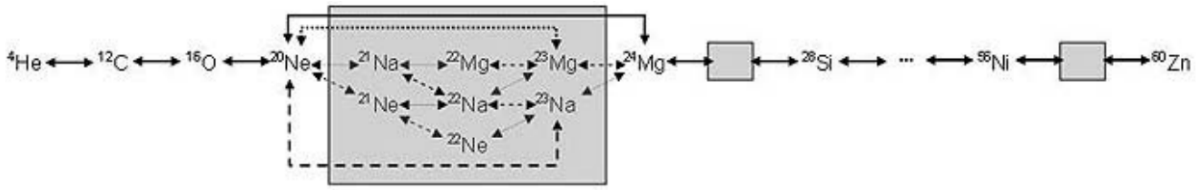

Figure 5: Scheme of the nuclear reactions network Net86 ([4]). The reactions are represented by the arrows: (p,γ) thin solid arrows, (n,γ) small dotted arrows, (α,γ) thick solid arrows, (α,p) long-dashed arrows, and (α,n) large dotted arrows.

Net86 is the updated moderate-sized nuclear network able to work with 86 different isotopes from ^{4}He to ^{60}Zn, including protons and neutrons. The net is organized into groups around an α-chain and the reactions between the isotopes are represented in Fig. 5. This net also includes triple alpha and binary reactions of carbon and oxygen, as Net14 did. It is expected that Net86 provides a much realistic nuclear energy release and nucleosynthesis. Nevertheless, although adequately tested in [4], it has never been incorporated to any hydrodynamical code since.

3.3 Net87. Electron Captures

This last net, Net87, is in fact an update of Net86 where the addition of electron captures on protons have been implemented; here, the molar fraction of electrons Y_e is not kept constant and hence they are treated as a whole new specie.

The process of electron capture takes place only in high-density environments, when the Fermi energy of degenerate electrons is enough to surpass the threshold of the negative Q-value of the capture reaction, which is $Q = (m_p + m_e - m_n - m_{\nu_e})c^2 = -0.782$ MeV. In the case of a WD, these conditions are only met at the core, where densities higher than $\rho \sim 10^7$ g/cm^3 are reached.

There are two main effects of electron captures during a SN Ia:

- **Pressure decrease.** Since a white dwarf's only opposition to collapse is the pressure exerted by the degenerate electrons, the reduction of the fraction of electrons Y_e results in a decrease of the pressure, changing the environment of the combustion and altering the outcome. Actually, for large enough densities the pressure is reduced drastically and may lead to a collapse of the star.

- **The neutronization of the isotopes.** After an electron capture, one proton of the target isotope is irreversibly converted into a neutron (the inverse reaction of electron capture takes place at a negligible rate since the neutrino-neutron collision is highly improbable). This process changes the nucleosynthesis yields, increasing the number of more neutronized isotopes and, in general, altering the composition of the ejected material after the explosion.

The topic of electron capture in degenerate matter is a very complicated subject. In this work

we have only considered electron-captures on free protons. The reason for that is twofold:

1. Previous work [15] have shown that around ~60% of the electron captures are produced on free protons.

2. The electron capture rate on free protons is well known whereas the capture rate on heavy nuclei suffers from a much larger uncertainty.

Nonetheless, the treatment of electrons as an independent new specie allows for easier future additions of captures on other nuclei, if needed.

The electron capture reaction on protons can be expressed as $p^+ + e^- \xrightarrow{\lambda_p} n + \nu_e$. The outcome of the reaction is a neutron and an electronic neutrino and the rate λ_p has been computed according to the expressions given by Hansen [8].

$$\lambda_p = 4.7 \times 10^{-4} \left(\frac{\mu^5}{5} + 8 \times 10^{-3} \mu^3 {T_9}^2 + 3.2 \times 10^{-3} {T_9}^5 \right) s^{-1} \tag{8}$$

$$\mu = min \left(10^{-2} (\rho Y_e)^{\frac{1}{3}}, 6 \times 10^{-6} \rho Y_e {T_9}^{-2} \right) \tag{9}$$

The term μ corresponds to the chemical potential of electrons and it is strongly dependent on the density, which makes captures only noticeable in high density scenarios such as C+O combustions. It is important to mention that this expressions are good approximations within a certain range of conditions, this is $T_9 \gtrsim 10$ or $\beta\mu \gtrsim 1$, where $\beta = \frac{m_e c^2}{kT}$.

The neutronization of the system causes a reduction of Y_e and most of the energy lost in the degenerate electron gas is radiated in the produced neutrinos that escape the nuclei. The rate of the neutrino energy is computed by the following expression:

$$\epsilon_p \lambda_p = 3.8 \times 10^{-4} (\frac{\mu^6}{6} + 6 \times 10^{-2} \mu^4 {T_9}^2 + 3.2 \times 10^{-3} T_9) \; s^{-1} \tag{10}$$

The implementation of electron captures in Net87 is carried out by adding the new term into both protons and neutrons equations, as well as adding three new terms to the energy equation 7. Also, a new equation has to be added to track the evolution of the electron molar fraction Y_e (see equation 13. Thus, the new set of equations are:

$$\frac{dY_p}{dt} = ... - \lambda_p Y_p \tag{11}$$

$$\frac{dY_n}{dt} = ... + \lambda_p Y_p \tag{12}$$

$$\frac{dY_e}{dt} = -\lambda_p Y_p \tag{13}$$

$$\sum_k Q_k \Delta Y_k + B_{pn} \Delta Y_e - \dot{v} \Delta t = \frac{\partial U}{\partial T} \Delta T + \sum_k \frac{\partial U_{ions}}{\partial Y_k} \Delta Y_k + \frac{\partial U_e}{\partial Y_e} \Delta Y_e \tag{14}$$

Equation 14 is the isochoric energy equation 7 with the addition of the new electron capture terms. The first new term $B_{pn} \Delta Y_e$ accounts for the mass defect of protons with respect to neutrons, where $B_{pn} = 0.782\,\text{MeV}$. This term is necessary since the nets work with both particles

having the same mass equal to 1 amu [7]. The second term is $-\dot{\nu}\Delta t = \epsilon_p \lambda_p Y_p \Delta t$, which accounts for the energy taken away by the neutrinos.They are supposed to freely abandon the star and thus, that energy is simply lost from the system. The third and last term $\frac{\partial U_e}{\partial Y_e}\Delta Y_e$ is added to take into account the loss of internal energy of the degenerate gas regarding the reduction of the number of electrons. In adiabatic compression or expansion the change of the internal energy due to a variation in the density has to be added (see equation 4).

4 Performance

4.1 Computational Overhead

The main computational load when calling the subroutines consists of two contributions: the calculation of the rates and their derivatives, and the solving of the linearized system. Small nuclear nets are ideal for performing fast simulations due to their reduced number of isotopes; Net14 for example, works with alpha capture reactions, which results in the calculation of only 17 rates and 13 inverse rates and their respective derivatives. The solving of the system is then carried out by inverting the 15x15 matrix of the system.

However, small nets provide only an approximate value of the released nuclear energy (within a 20% of the value estimated with larger networks) and a rough idea of the nucleosynyhetic yields. Moderate-size nets such as Net86 and Net87 are more sophisticated and provide far more accurate estimation of the released energy and synthesized yields. Such enhancement is, of course, not for free and an increment in the computational load is expected.

The main problem of using large nuclear nets is indeed the process of inverting the matrix. Standard routines to solve linear systems scale $\sim N^3$ and are expensive. At present, Net14-86-87 make use of the special method explained in [14] which is specially addressed to solve sparse matrices linked to nuclear networks with a cost $\sim N^2$. It is therefore interesting to investigate the ratio between the time invested in computing the rates to that used to invert the matrix. This is done in our Table 1.

	Rates and Derivatives	Sparse Matrix	Load Matrix/Load Rates
Net14	$(16 + inverse) \times 2$	15×15	2.51
Net86	$(157 + inverse) \times 2$	87×87	12.04
Net87	$(159 + inverse) \times 2$	88×88	12.19

Table 1: Main overhead of the nets. Columns show the number of rates and derivatives to be computed, the dimensions of the matrix of the linearized system, and the cost ratio between both wall-clock times.

Table 1 shows for each of the nets where the main computational load falls on. The most remarkable result is the fast escalation of the cost of the inversion process when increasing the size of the network. Nonetheless, this is not unexpected because the cost of the rates grows linearly, while the matrix does not, as mentioned before. This results suggests that a more efficient algorithm to invert the matrix would be of great interest.

The execution times when calling the nets increases with the number of variables, we can expect a relation of the type: $t_{14} < t_{86} < t_{87}$. In order to measure this, we performed for each of the nets a high-density C+O combustion but each time-step was performed 100 times to average

the execution time value and obtain a better result. Thus, the following relations were found:

$$\frac{t_{86}}{t_{14}} = 22.232 \qquad \frac{t_{87}}{t_{86}} = 1.114 \qquad \frac{t_{87}}{t_{14}} = 24.775$$

The cost of using the moderately-sized Net86 is more than 22 times larger than that of using the small net14; including electron captures into Net86 suppose a 11.4% increase on the computational load. It is important to mention that these results are meant to represent the rough subroutine comparison with 1 iteration in the solving process (i.e. without an iterative solver). In the following section, a more representative study is made including a complete iterative solver (Newton-Raphson method) and taking into account that each network may converge differently.

4.2 Implementation of an iterative solver. Newton-Raphson Method

The implementation of an iterative Newton-Raphson (NR) method is a useful resource for finding better and more accurate solutions to the systems of equations that the nets work with, especially when dealing with implicit or semi-implicit systems. Improving the accuracy makes each state of the evolution of the system more reliable, allowing greater time-steps and hence covering the whole combustion process faster. However, implementing the NR method requires multiple iterations for each time-step, which implies from twice to six or seven times the cost of an ordinary call to the subroutine.

In order to study the quality of the implementation of this iterative method the conservation of mass δ can be used as a marker of the accuracy. Taking the sum of abundances of every isotope as $m_T = 1 = \sum X_k$, the conservation of mass is computed as $\delta = \|m_T - 1\|$. In net87 for example, if $\delta < 10^{-5}$ is wanted to be fulfilled during a C+O combustion at $\rho_9 = 2$, the time-control parameter on temperature α can't go much higher than 1.25×10^{-5} without Newton-Raphson (i.e. $\Delta t = \alpha \frac{T}{\Delta T} = 1.25 \times 10^{-5} \frac{T}{\Delta T}$).

	$\delta < 10^{-5}$				$\delta < 10^{-3}$			
	Net14		Net87		Net14		Net87	
	No NR	NR	No NR	NR	No NR	NR	No NR	NR
α	4.33(-5)	1.82(-2)	1.25(-5)	1.98(-2)	4.51(-5)	1.89(-2)	4.13(-4)	2.20(-2)
Steps	371691	2322	915917	2079	353806	2320	26549	2066
Iter.	371691	6934	915917	5864	353806	6940	26549	5752
ips	1	2.986	1	2.821	1	2.991	1	2.784

Table 2: Maximum time-control parameter α, number of time-steps of the integration process, total number of Newton-Raphson iterations and mean number of iterations per time-step (ips) for both $\delta < 1 \times 10^{-3}$ and $\delta < 1 \times 10^{-5}$, during a $\rho_9 = 2$ carbon and oxygen combustion with adiabatic expansion.

The results shown in Table 2 demonstrate that using an iterative solver in high-density combustion, where temperatures around $T_9 = 10$ are reached, is absolutely necessary in order to maintain a reasonable conservation of mass without having to take very small time-steps, increasing the computation time and lowering the performance. Even though the iterations per step are increased, the addition of NR allows using large time-steps without compromising the accuracy of the solutions and saving computational time.

For low-density combustion, the maximum temperature is not so high and, therefore, the mass

is better conserved than in the high-density case. Nevertheless, including NR is crucial for achieving much more accuracy with extended time-steps and improving general performance when using the nets, as it did for high-density combustion.

As advanced in the previous section, we can repeat the comparison of the computational costs of each net but now including the Newton-Raphson method into each net. We performed a C+O combustion at density $\rho_9 = 2$ and a time-step control parameter $\alpha = 0.01$. The new subroutine-call time ratios are:

$$\frac{t'_{86}}{t'_{14}} = 24.775 \qquad \frac{t'_{87}}{t'_{86}} = 0.958 \qquad \frac{t'_{87}}{t'_{14}} = 23.739$$

These values were obtained by averaging in the same way as in the previous section. They are very interesting since they show the efficiency of the convergence of the NR in each case. For further understanding of these results, it is necessary to compute the mean number of iterations per time-step of each of the nets, which we will call ips_{14}, ips_{86} and ips_{87}. Moreover, putting in comparison these values with those computed in the previous section, i.e. without including NR:

$$\frac{t'_{86}/t'_{14}}{t_{86}/t_{14}} = \frac{24.775}{22.232} = 1.114 \sim 1.088 = \frac{3.6901}{3.3902} = \frac{ips_{86}}{ips_{14}}$$

$$\frac{t'_{87}/t'_{86}}{t_{87}/t_{86}} = \frac{0.958}{1.114} = 0.860 \sim 0.868 = \frac{3.2044}{3.6901} = \frac{ips_{87}}{ips_{86}}$$

$$\frac{t'_{87}/t'_{14}}{t_{87}/t_{14}} = \frac{23.739}{24.775} = 0.958 \sim 0.945 = \frac{3.2044}{3.3902} = \frac{ips_{87}}{ips_{14}}$$

As it is shown above, including the iterative solver makes Net87 faster than Net86 despite the increase of calculations due to the addition of electron captures. Net87 takes less iterations than Net86 to converge during the combustion process, possibly caused by the different thermodynamic evolution. Making this same study on other scenarios, such as low density He-burning, might provide different results since the convergence process is truly dependent on the current state of the combustion.

4.3 Semi-Implicit Scheme

When discretizing the system of equations, the parameter theta is used to determine the degree of implicitness of the scheme. Sometimes, nucleosynthesis simulations are performed in explicit schemes ($\theta = 0$), which are actually very comfortable when integrating in time since it is not necessary to invert any matrix or use iterative solvers. However, the reliability of the results may not be as desired due to the intrinsic instability of explicit schemes.

Using an implicit scheme ($\theta = 1$) assures stability along the whole integration at the cost of complicating the system of equations. However, the use of a fully implicit scheme may err to over-stability and also lead to inaccurate results in some scenarios. Net14 for example was originally used in a fully implicit scheme due to some instabilities in the NSE regime.

An intermediate approach with $\theta = 0.5$, called a semi-implicit scheme, provides the most accurate results when integrating the system. This improvement is due to the fact that the integration is made up to second order, whereas taking fully explicit or implicit schemes is only first order.

In order to visualize this, some simulations were performed using different values of the parameter theta:

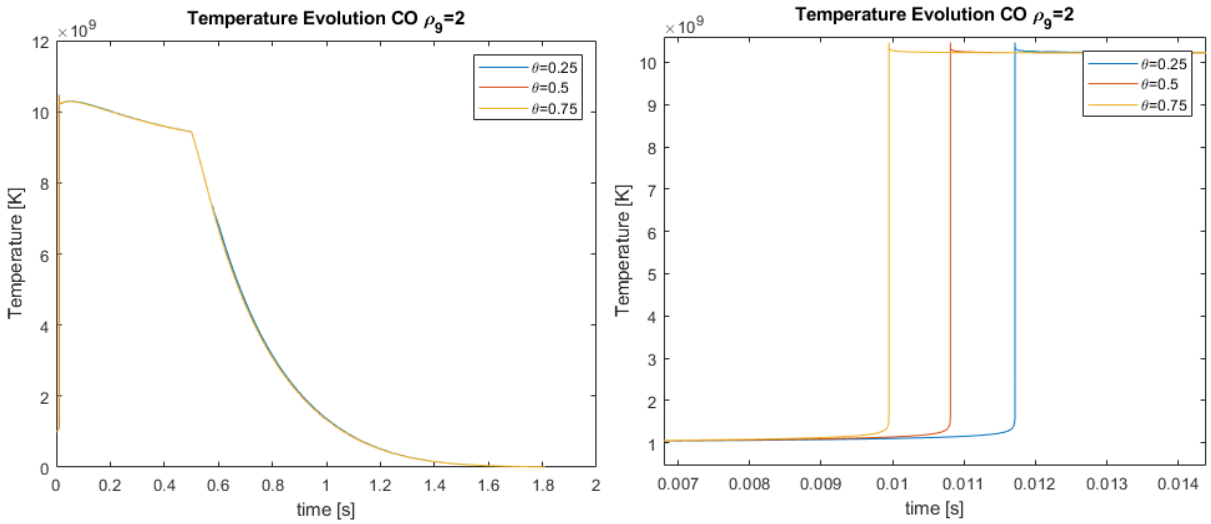

Figure 6: Temperature Evolution of a C+O combustion at $\rho_9 = 2$ (Left). Detonation Time (Right).

The left hand figure in 6 shows the temperature evolution for $\theta = 0.25, 0.5, 0.75$ on a C+O combustion with adiabatic expansion. The three values lead to almost indistinguishable graphs, with good temperature values and decent mass conservation. Nonetheless, the right hand figure shows a zoomed in version focused on the time of nuclear runaway, when T rises dramatically in a tiny period of time. Each of the values of theta yields a different time for the explosion event, larger or smaller for explicit or implicit schemes, respectively.

This phenomenon is easily explained by just looking at the following fact during the burning phase:

$$T^n \leq T^{n+\theta} \leq T^{n+1}$$

$$r_{ij}(T^n) \leq r_{ij}(T^{n+\theta}) \leq r_{ij}(T^{n+1})$$

Implicit methods evaluate at the future state, where the temperature has increased with respect to the present value, making the reaction rates higher and consequently advancing the explosion time. The opposite occurs for explicit schemes, where the evaluation of the variables is done on the present values, lower than that of the future state. A semi-implicit scheme with $\theta = 0.5$ yields the most accurate integration, for the evaluation takes place at mean values between both present and future states.

As a side note, it is good to mention that the full potential of using non-explicit schemes is achieved when paired with an iterative solver, since the cut-off at just 1 iteration usually provides inaccurate approximations to the solution of the system.

5 Results

With the implementation already finished, including the iterative Netwon-Raphson solver, the semi-implicit scheme, and the optimal tuning of the parameters, it is time to compare the results that the three nuclear networks provide in some different scenarios. The following sections are going to focus on the outcome of the nets in high density 50%C+50%O and 49%C+49%O+2%Ne combustions, as well as low density 100%He combustions. In addition to these scenarios related to SN Ia explosions, we have also explored a crucial process to understand Type II supernova explosions: the high temperature silicon burning.

5.1 High Density 50%C+50%O Combustion

At the core of white dwarfs, the ignition of carbon and oxygen occurs at densities ranging from $\rho_9 = 0.1$ to $\rho_9 = 2$. The explosive ignition process of carbon takes place in a much lower time scale than the hydrodynamical time so that temperatures of the order of 9-10 billion degrees are reached almost instantaneously.

5.1.1 Temperature, Pressure and Released Energy

For this case of high-density combustion, a more profound study on the evolution of temperature, pressure, and the released nuclear energy has been carried out in order to put in comparison not only the nucleosynthesis of the nets but also their thermodynamical performance.

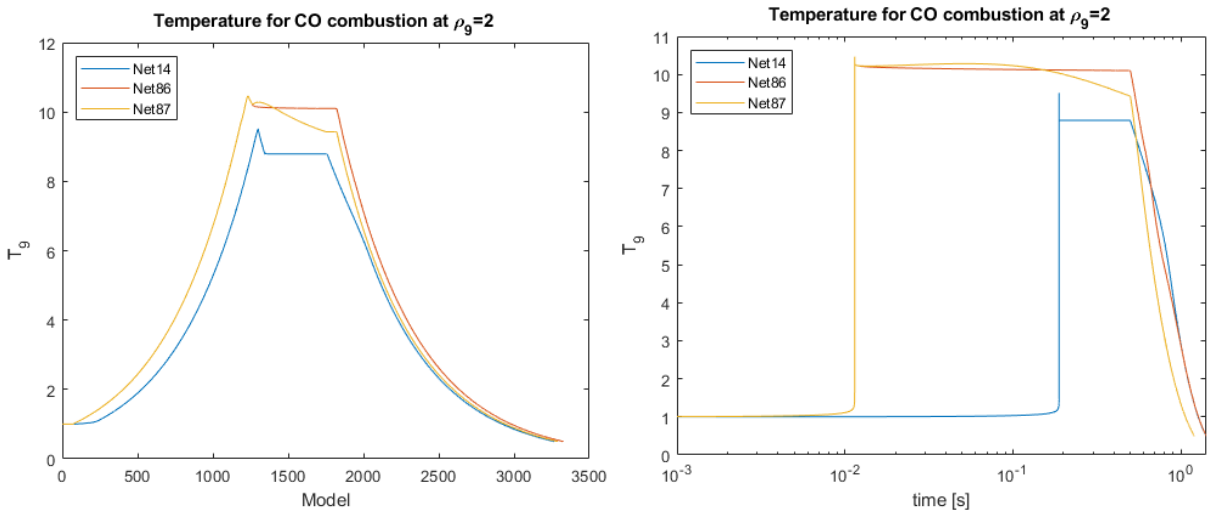

Figure 7: Temperature evolution for a carbon and oxygen combustion at initial density $\rho_9 = 2$, for each of the three nets.Note the plateau around model 1500, which corresponds to the complete nuclear statistical equilibrium of the burnt material.

It is worth noting the reduction of pressure gas shown in Figure 8 during the NSE due to the electron captures in Net87, which could have an impact in the dynamics of the explosion. Also, the reduction of the temperature in 7 is explained by the fact that the electron capture reaction itself is endoenergetic, in addition to the energy lost by the emission of neutrinos.

The nuclear energy released during combustion is very different depending on the used Net, as shown in Figure 9. While both Net14 and Net86 provide very similar evolutions, Net87, the network that includes electron captures, presents a very distinctive behaviour. There are two

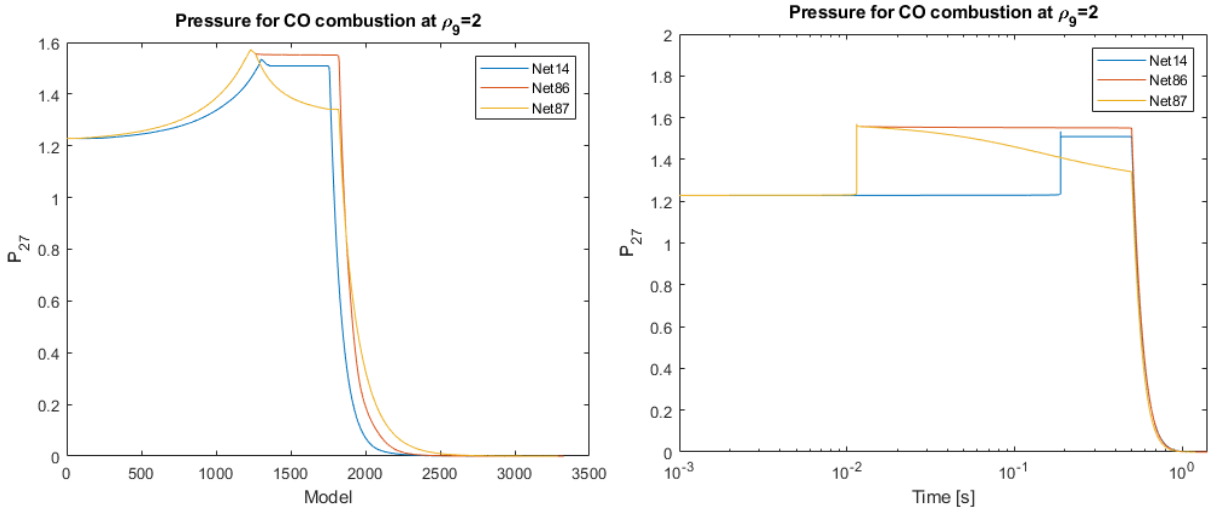

Figure 8: Same as figure 7 but for the pressure

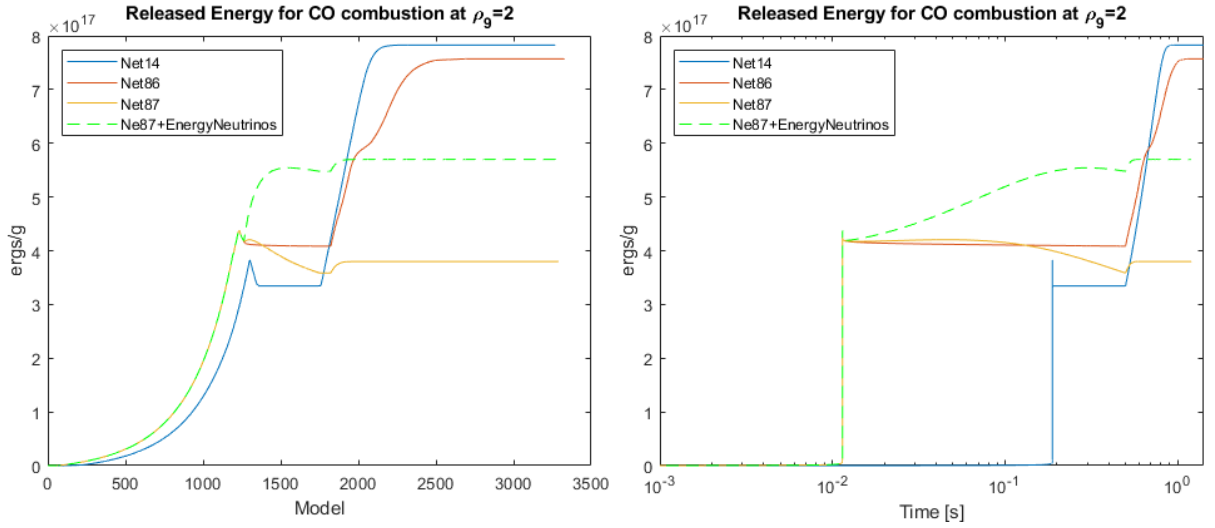

Figure 9: Same as figure 7 and 8 but for the released nuclear energy and energy-loss due to neutrinos

main causes of this, the first is that, with electron captures, some of the energy is lost in the emission of neutrinos. The second is that nuclear reactions involving neutrons (more abundant in Net87 due to neutronization of the system) release less energy than reactions involving protons (more abundant in Net86). This fact is related to the difference in charge of both protons and neutrons, since neutrons are not electrically charged they do not have to overcome a coulombic potential barrier and their capture on nuclei is energetically more feasible that in the case of protons, which do have charge.

5.1.2 Nucleosynthesis Yields of C+O combustion

	Net87						Net86					
	$\rho_9 = 2$		$\rho_9 = 1$		$\rho_9 = 0.1$		$\rho_9 = 2$		$\rho_9 = 1$		$\rho_9 = 0.1$	
	NSE	Freeze	NSE	Freeze	NSE	Freeze	NSE	Freeze	NSE	Freeze	NSE	Freeze
T_9	9,4	9,9(-3)	9,3	1,0(-2)	7,3	1,0(-2)	10,0	1,0(-2)	9,4	1,0(-2)	7,0	1,0(-2)
Pr_{27}	1,3	2,5(-9)	6,0(-1)	5,3(-10)	4,6(-2)	3,1(-11)	1,6	1,4(-10)	6,6(-1)	1,1(-10)	4,4(-2)	3,0(-11)
Y_e	0,4564	0,4562	0,4661	0,4654	0,4939	0,4934	0,5000	0,5000	0,5000	0,5000	0,5000	0,5000
^{1}H	1,3(-3)	0	6,2(-3)	0	2,3(-2)	1,3(-14)	4,2(-2)	5,0(-9)	4,1(-2)	5,1(-9)	3,2(-2)	7,5(-9)
n	5,6(-2)	5,5(-2)	4,1(-2)	3,6(-2)	1,6(-3)	0	1,1(-2)	0	9,0(-3)	0	2,7(-4)	0
^{4}He	4,2(-4)	9,6(-5)	8,1(-4)	3,1(-3)	9,8(-4)	1,3(-2)	3,5(-3)	7,3(-3)	1,3(-3)	8,1(-3)	5,3(-4)	1,2(-2)
^{12}C	5,1(-13)	2,6(-9)	1,0(-12)	5,6(-6)	4,4(-13)	1,9(-5)	1,3(-10)	9,8(-6)	3,5(-12)	1,1(-5)	5,1(-12)	1,8(-5)
^{16}O	1,9(-15)	1,6(-12)	2,3(-15)	3,2(-9)	3,3(-15)	1,2(-8)	8,0(-13)	5,6(-9)	1,8(-14)	6,5(-9)	9,3(-13)	1,1(-8)
^{20}Ne	0	0	0	0	0	7,5(-9)	0	3,0(-9)	0	3,6(-9)	1,2(-14)	6,4(-9)
^{21}Ne	0	0	0	0	0	5,6(-8)	0	2,3(-7)	0	2,1(-7)	0	1,3(-7)
^{22}Ne	6,1(-15)	2,3(-8)	0	3,3(-4)	0	0	0	0	0	0	0	0
^{21}Na	0	0	0	0	0	0	0	0	0	0	0	0
^{22}Na	0	0	0	0	0	4,1(-14)	0	4,8(-10)	0	6,0(-10)	0	1,3(-9)
^{23}Na	8,1(-15)	3,0(-9)	0	5,9(-7)	0	1,6(-8)	8,1(-15)	1,7(-12)	5,3(-15)	1,7(-12)	1,2(-14)	1,6(-12)
^{22}Mg	0	0	0	0	0	3,5(-11)	0	6,3(-6)	0	7,6(-6)	0	1,4(-5)
^{23}Mg	0	0	0	0	0	0	0	0	0	0	0	0
^{24}Mg	6,4(-15)	0	4,5(-15)	0	3,7(-15)	7,7(-8)	9,5(-14)	2,5(-8)	6,7(-14)	3,2(E-8)	1,5(-12)	6,3(-8)
^{25}Mg	0	0	0	0	0	2,6(-8)	2,7(-4)	1,2(-7)	6,5(-15)	1,1(E-7)	6,2(-14)	6,5(-8)
^{26}Mg	1,9(-12)	1,8(-10)	2,4(-13)	4,4(-5)	0	0	3,2(-3)	0	1,0(-13)	0	4,6(-14)	0
^{25}Al	0	0	0	0	0	0	6,2(-14)	0	1,6(-14)	0	5,7(-14)	0
^{26}Al	0	0	0	0	0	1,5(-13)	0	1,8(-9)	0	2,2(-9)	3,7(-15)	5,7(-9)
^{27}Al	1,5(-12)	8,7(-12)	4,7(-13)	1,6(-8)	2,5(-14)	1,5(-6)	3,3(-12)	2,0(-9)	1,1	2,4(-9)	2,3(-12)	3,6(-9)
^{26}Si	0	0	0	0	0	1,9(-11)	0	1,6(-6)	0	2,0(-6)	0	4,2(-6)
^{27}Si	6,0(-14)	0	1,7(-14)	0	0	0	1,1(-13)	0	4,7(-14)	0	1,2(-13)	0
^{28}Si	1,4(-12)	0	1,3(-12)	0	1,9(-12)	4,9(-7)	3,6(-11)	3,2(-8)	1,7(-11)	4,1(-8)	4,9(-10)	8,6(-8)
^{29}Si	0	0	3,8(-15)	0	5,9(-15)	9,4(-10)	1,4(-12)	5,6(-9)	3,1(-13)	4,8(-9)	2,2(-12)	2,8(-9)
^{30}Si	9,5(-10)	3,5(-11)	1,6(-10)	1,3(-4)	3,8(-12)	0	2,0(-10)	0	6,9(-11)	0	7,3(-11)	0
^{29}P	2,9(-13)	0	2,7(-13)	0	9,8(-14)	0	1,5(-11)	0	3,7(-12)	0	1,7(-11)	0
^{30}P	0	0	0	0	4,4(-15)	1,6(-11)	3,6(-13)	1,2(-8)	1,0(-13)	1,5(-8)	1,0(-12)	3,5(-8)
^{31}P	1,1(-10)	4,1(-14)	4,9(-11)	3,6(-10)	6,6(-12)	1,3(-6)	3,9(-10)	8,3(-11)	1,2(-10)	9,8(-11)	3,0(-10)	1,4(-10)
^{30}S	0	0	0	0	0	2,9(-11)	4,0(-15)	1,2(-6)	0	1,5(-6)	6,5(-15)	3,3(-6)
^{31}S	2,5(-11)	0	9,5(-12)	0	1,2(-12)	0	6,6(-11)	0	2,3(-11)	0	9,6(-11)	0
^{32}S	4,7(-12)	0	5,4(-12)	0	8,3(-12)	1,7(-6)	2,0(-10)	5,1(-9)	7,4(-11)	6,8(-9)	9,6(-10)	1,5(-8)
^{33}S	6,5(-15)	0	1,9(-14)	0	2,9(-14)	7,6(-10)	8,6(-12)	3,7(-9)	1,7(-12)	3,2(-9)	4,6(-12)	2,0(-9)
^{34}S	1,2(-8)	1,4(-10)	2,8(-9)	7,2(-5)	1,2(-10)	1,2(-13)	3,7(-9)	0	1,3(-9)	0	1,3(-9)	0
^{33}Cl	1,5(-12)	0	1,8(-12)	0	7,5(-13)	6,0(-15)	1,1(-10)	0	2,7(-11)	0	5,4(-11)	0
^{34}Cl	0	0	6,0(-15)	0	9,4(-15)	1,9(-12)	2,3(-12)	1,7(-10)	5,1(-13)	2,3(-10)	1,9(-12)	5,6(-10)
^{35}Cl	7,6(-10)	1,1(-14)	4,3(-10)	2,3(-11)	8,2(-11)	2,6(-6)	3,8(-9)	7,2(-12)	1,2(-9)	8,8(-12)	2,1(-9)	1,4(-11)
^{34}Ar	0	0	0	0	0	3,0(-11)	2,1(-14)	8,2(-7)	3,5(-15)	1,0(-6)	1,0(-14)	2,0(-6)
^{35}Ar	1,9(-10)	0	9,6(-11)	0	1,5(-11)	0	7,9(-10)	0	2,5(-10)	0	5,2(-10)	0
^{36}Ar	2,9(-11)	0	4,4(-11)	0	8,8(-11)	3,1(-6)	1,6(-9)	4,9(-9)	6,6(-10)	5,5(-9)	5,7(-9)	8,9(-9)
^{37}Ar	2,7(-14)	0	1,0(-13)	0	2,6(-13)	3,4(-9)	4,4(-11)	1,3(-8)	1,0(-11)	1,1(-8)	2,3(-11)	8,0(-9)
^{38}Ar	1,4(-7)	3,4(-9)	4,1(-8)	3,6(-5)	3,0(-9)	2,5(-13)	5,0(-8)	0	2,1(-8)	0	2,1(-8)	0
^{37}K	8,7(-12)	0	1,4(-11)	0	9,3(-12)	2,7(-13)	8,1(-10)	0	2,3(-10)	0	3,8(-10)	0
^{38}K	9,1(-15)	0	3,2(-14)	0	5,4(-14)	9,7(-14)	1,3(-11)	9,6(-12)	3,0(-12)	1,1(-11)	5,8(-12)	2,1(-11)
^{39}K	6,9(-9)	2,5(-13)	5,1(-9)	9,1(-12)	1,9(-9)	3,4(-6)	4,0(-8)	7,1(-12)	1,5(-8)	7,7(-12)	3,0(-8)	1,0(-11)
^{38}Ca	0	0	0	0	0	4,8(-12)	8,7(-14)	3,0(-7)	1,5(-14)	3,5(-7)	2,3(-14)	6,3(-7)
^{39}Ca	1,5(-9)	0	9,9(-10)	0	2,0(-10)	0	8,0(-9)	0	2,8(-9)	0	4,0(-9)	0
^{40}Ca	2,4(-10)	0	4,7(-10)	0	1,7(-9)	4,8(-5)	1,7(-8)	9,2(-6)	8,0(-9)	1,1(-5)	7,0(-8)	2,5(-5)
^{41}Ca	3,7(-14)	0	1,8(-13)	0	2,6(-13)	2,4(-10)	9,8(-11)	1,1(-9)	2,1(-11)	1,0(-9)	1,2(-11)	9,2(-10)
^{42}Ca	1,2(-6)	2,6(-8)	4,5(-7)	5,2(-5)	3,0(-8)	1,0(-11)	6,4(-7)	0	2,6(-7)	0	1,3(-7)	0
^{41}Sc	2,9(-11)	0	5,7(-11)	0	3,0(-11)	1,0(-11)	4,0(-9)	0	1,1(-9)	0	7,0(-10)	0
^{42}Sc	5,6(-14)	0	2,5(-13)	0	5,7(-13)	0	1,1(-10)	4,4(-11)	2,7(-11)	5,3(-11)	3,8(-11)	1,2(-10)
^{43}Sc	3,2(-8)	6,9(-15)	2,9(-8)	7,9(-13)	6,4(-9)	1,3(-8)	2,9(-7)	8,6(-14)	1,0(-7)	8,6(-14)	5,5(-8)	8,0(-14)
^{42}Ti	0	0	0	0	0	0	3,6(-13)	1,6(-8)	5,9(-14)	1,9(-8)	3,8(-14)	3,2(-8)
^{43}Ti	1,5(-8)	0	1,2(-8)	0	3,8(-9)	9,2(-11)	9,9(-8)	0	3,9(-8)	0	4,7(-8)	0
^{44}Ti	4,0(-10)	0	1,0(-9)	0	2,2(-9)	2,8(-5)	2,4(-8)	2,8(-7)	1,9(-8)	3,4(-7)	4,6(-8)	7,0(-7)
^{45}Ti	7,1(-13)	0	4,7(-12)	0	1,1(-11)	9,5(-8)	1,3(-9)	1,7(-7)	5,8(-10)	1,7(-7)	3,0(-10)	1,6(-7)
^{46}Ti	2,8(-5)	1,7(-6)	1,4(-5)	2,6(-5)	2,5(-6)	9,4(-11)	8,7(-6)	0	8,8(-6)	0	6,8(-6)	0
^{45}V	3,1(-10)	0	8,4(-10)	0	7,2(-10)	6,0(-10)	2,9(-8)	5,5(-15)	1,7(-8)	4,6(-15)	1,0(-8)	0
^{46}V	1,2(-13)	0	7,1(-13)	0	1,9(-12)	1,8(-13)	1,5(-10)	1,4(-10)	8,2(-11)	1,6(-10)	6,4(-11)	3,8(-10)
^{47}V	9,1(-7)	1,8(-12)	1,1(-6)	5,1(-13)	6,5(-7)	4,8(-7)	5,1(-6)	2,7(-12)	4,2(-6)	2,9(-12)	3,6(-6)	4,4(-12)
^{46}Cr	0	0	0	0	0	1,2(-10)	8,3(-13)	1,2(-5)	2,6(-13)	1,5(-5)	1,2(-13)	3,0(-5)
^{47}Cr	1,1(-7)	0	1,2(-7)	0	4,5(-8)	2,9(-11)	5,0(-7)	0	4,0(-7)	0	3,0(-7)	0
^{48}Cr	1,3(-8)	0	4,2(-8)	0	1,9(-7)	8,3(-5)	1,0(-6)	1,6(-6)	8,9(-7)	1,9(-6)	2,6(-6)	3,6(-6)
^{49}Cr	2,5(-11)	0	2,1(-10)	0	1,3(-9)	5,5(-7)	5,7(-8)	6,9(-7)	3,0(-8)	7,1(-7)	2,7(-8)	7,5(-7)
^{50}Cr	2,8(-3)	6,3(-4)	1,8(-3)	2,9(-5)	7,6(-4)	3,5(-11)	1,2(-3)	0	1,3(-3)	0	1,5(-3)	0
^{49}Mn	1,6(-8)	0	5,5(-8)	0	1,1(-7)	6,4(-9)	2,0(-6)	4,3(-14)	1,3(-6)	3,5(-14)	1,1(-6)	1,7(-14)
^{50}Mn	4,3(-12)	0	3,3(-11)	0	1,7(-10)	1,9(-11)	7,6(-9)	1,2(-8)	4,3(-9)	1,4(-8)	4,1(-9)	2,2(-8)
^{51}Mn	5,0(-5)	7,4(-10)	8,0(-5)	3,4(-13)	1,2(-4)	1,6(-7)	3,7(-4)	1,2(-12)	3,4(-4)	1,3(-12)	4,7(-4)	1,9(-12)
^{50}Fe	0	0	2,5(-14)	0	1,5(-13)	4,5(-11)	6,5(-11)	3,1(-5)	2,0(-11)	3,8(-5)	6,9(-12)	7,9(-5)
^{51}Fe	6,1(-6)	0	8,7(-6)	0	8,8(-6)	4,2(-9)	3,8(-5)	0	3,4(-5)	0	4,2(-5)	0
^{52}Fe	4,2(-7)	0	1,7(-6)	0	1,6(-5)	1,6(-4)	4,6(-5)	7,7(-5)	4,2(-5)	9,1(-5)	1,5(-4)	1,7(-4)
^{53}Fe	3,9(-10)	0	4,1(-9)	0	4,8(-8)	2,0(-6)	1,2(-6)	2,5(-6)	6,7(-7)	2,5(-6)	6,4(-7)	2,8(-6)
^{54}Fe	1,3(-1)	1,0(-1)	1,1(-1)	9,4(-3)	1,0(-1)	9,6(-10)	8,0(-2)	0	9,1(-2)	0	1,4(-1)	0
^{53}Co	4,4(-7)	0	1,9(-6)	0	7,8(-6)	2,5(-7)	7,9(-5)	3,6(-12)	5,2(-5)	3,1(-12)	5,2(-5)	1,9(-12)
^{54}Co	5,2(-11)	0	4,9(-10)	0	4,5(-9)	3,5(-13)	1,4(-7)	7,8(-9)	7,5(-8)	8,3(-9)	7,3(-8)	1,1(-8)
^{55}Co	1,4(-3)	4,7(-8)	2,8(-3)	3,8(-11)	9,8(-3)	8,4(-7)	1,4(-2)	3,3(-11)	1,3(-2)	3,6(-11)	2,8(-2)	4,7(-11)
^{54}Ni	8,6(-15)	0	1,9(-13)	0	2,3(-12)	5,8(-13)	5,6(-10)	6,3(-6)	1,8(-10)	7,2(-6)	7,1(-11)	1,1(E-5)

	Net87						Net86					
	$\rho_9 = 2$		$\rho_9 = 1$		$\rho_9 = 0.1$		$\rho_9 = 2$		$\rho_9 = 1$		$\rho_9 = 0.1$	
	NSE	Freeze	NSE	Freeze	NSE	Freeze	NSE	Freeze	NSE	Freeze	NSE	Freeze
^{55}Ni	2,6(-4)	0	4,7(-4)	0	9,1(-4)	3,8(-7)	2,4(-3)	0	2,1(-3)	0	3,1(-3)	0
^{56}Ni	6,6(-6)	0	3,4(-5)	0	7,3(-4)	4,3(-1)	9,9(-4)	6,9(-1)	9,5(-4)	7,0(-1)	4,9(-3)	7,1(-1)
^{57}Ni	3,4(-10)	0	4,2(-9)	0	1,8(-8)	5,6(-10)	2,4(-6)	1,5(-2)	8,4(-7)	1,5(-2)	1,4(-7)	1,4(-2)
^{58}Ni	8,0(-1)	8,4(-1)	8,2(-1)	9,5(-1)	8,3(-1)	3,5(-1)	7,7(-1)	1,9(-9)	7,8(-1)	1,5(-9)	7,2(-1)	7,5(-10)
^{57}Cu	1,7(-6)	0	8,9(-6)	0	3,1(-5)	4,5(-6)	5,3(-4)	1,1(-2)	2,9(-4)	1,1(-2)	1,3(-4)	1,1(-2)
^{58}Cu	6,0(-10)	0	7,0(-9)	0	7,6(-8)	3,4(-14)	2,6(-6)	3,6(-8)	1,2(-6)	3,3(-8)	8,1(-7)	2,9(-8)
^{59}Cu	1,8(-3)	9,5(-12)	4,5(-3)	6,7(-12)	6,8(-3)	7,3(-3)	3,8(-2)	4,1(-7)	2,6(-2)	3,5(-7)	1,1(-2)	2,0(-7)
^{58}Zn	2,4(-14)	0	6,3(-13)	0	5,6(-12)	0	2,7(-9)	6,7(-11)	7,0(-10)	5,2(-11)	1,0(-10)	2,2(-11)
^{59}Zn	3,0(-3)	0	6,8(-3)	0	2,4(-2)	5,9(-2)	3,9(-2)	1,4(-2)	3,6(-2)	1,4(-2)	5,4(-2)	1,4(-2)
^{60}Zn	1,4(-6)	0	8,0(-6)	0	3,8(-5)	1,4(-1)	4,6(-4)	2,6(-1)	2,8(-4)	2,6(-1)	1,3(-4)	2,4(-1)

Table 3: Net86 and Net87 Nucleosynthesis yields of C+O burning for $\rho_9 = 2, 1, 0.1$, before the adiabatic expansion (NSE) and after the expansion (Freeze-out). Relevant information concerning achieved temperatures, pressures and neutronization, as well as on the more abundant nuclei are highlighted in different colors (temperature and pressure in yellow, Y_e in orange and isotopes abundances in blue).

	Net14					
	$\rho_9 = 2$		$\rho_9 = 1$		$\rho_9 = 0.1$	
	NSE	Freeze	NSE	Freeze	NSE	Freeze
T_9	8,8	1,0(-2)	8,2	9,9(-3)	6,5	9,9(-3)
Pr_{27}	1,5	1,4(-10)	6,3(-1)	1,1(-10)	4,1(-2)	3,0(-11)
Ye	0,5000	0,5000	0,5000	0,5000	0,5000	0,5000
^{4}He	2,8(-1)	5,3(-9)	2,7(-1)	7,8(-8)	1,8(-1)	2,4(-4)
^{12}C	5,2(-5)	3,3(-12)	4,2(-5)	2,2(-12)	1,2(-5)	8,8(-10)
^{16}O	1,2(-4)	4,9(-11)	1,0(-4)	4,2(-12)	3,1(-5)	7,0(-13)
^{20}Ne	1,0(E-5)	9,0(-14)	6,7(-6)	6,1(-14)	9,4(-7)	2,6(-13)
^{24}Mg	3,6(-4)	1,8(-10)	3,0(-4)	8,4(-12)	1,0(-4)	2,2(-12)
^{28}Si	2,1(-2)	1,6(-4)	2,4(-2)	3,2(-5)	2,7(-2)	2,1(-11)
^{32}S	2,4(-2)	1,1(-3)	2,7(-2)	4,7(-4)	3,3(-2)	3,0(-10)
^{36}Ar	2,3(-2)	2,1(-3)	2,5(-2)	1,6(-3)	2,6(-2)	3,3(-6)
^{40}Ca	2,8(-2)	1,1(-2)	3,0(-2)	1,1(-2)	3,5(-2)	1,5(-3)
^{44}Ti	9,2(-3)	7,9(-5)	8,1(-3)	1,6(-4)	3,2(-3)	5,7(-3)
^{48}Cr	4,1(-2)	2,3(-3)	3,7(-2)	2,1(-3)	2,1(-2)	2,0(-3)
^{52}Fe	1,7(-1)	4,3(-2)	1,7(-1)	4,0(-2)	1,3(-1)	2,6(-2)
^{56}Ni	3,9(-1)	9,4(-1)	4,0(-1)	9,4(-1)	5,4(-1)	9,6(-1)
^{60}Zn	5,7(-3)	3,0(-7)	3,7(-3)	6,7(-7)	6,8(-4)	1,6(-4)

Table 4: Net14 Nucleosynthesis yields of C+O burning for $\rho_9 = 2, 1, 0.1$, before the adiabatic expansion (NSE) and after the expansion (Freeze-out).

Tables 3 and 4 show the abundances of the resulting isotopes after the combustion, once the nuclear statistical equilibrium is reached and after the adiabatic expansion that follows the explosion. One of the most remarkable results is the change of abundances of nickel: the addition of electron captures on Net87 produces a drastically shifting to the more neutronized isotope ^{58}Ni, specially for the highest densities, compared to the typical dominance of ^{56}Ni on the other nets that do not incorporate electron captures in the scheme; this same effect is present at some extent for the other elements. The neutronization is also reflected on the decrease of Y_e, being major at greater densities since electron captures are favoured.

The comparison on the evolution of the species in figure 10 shows the disappearance of some isotopes due to the neutronization of the system in Net87, as well as the discrepancy of the abundances of some heavy elements when using Net86 instead of Net14. Another noticeable difference in the Net87 graph is the non-steadiness of the abundances in the NSE regime, the tracked isotopes are decreased due to the action of electron captures increasing their more neutronized variants, while the abundance of neutrons rises. Also, note the very different behaviour in the abundance of protons around the NSE between Net86 and Net87.

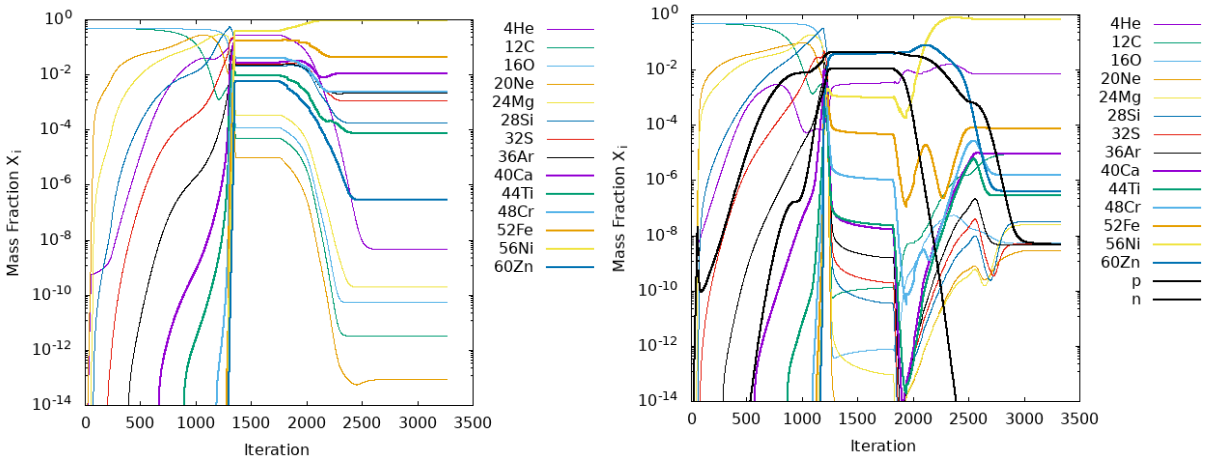

(*a*) *Net14* (*b*) *Net86*

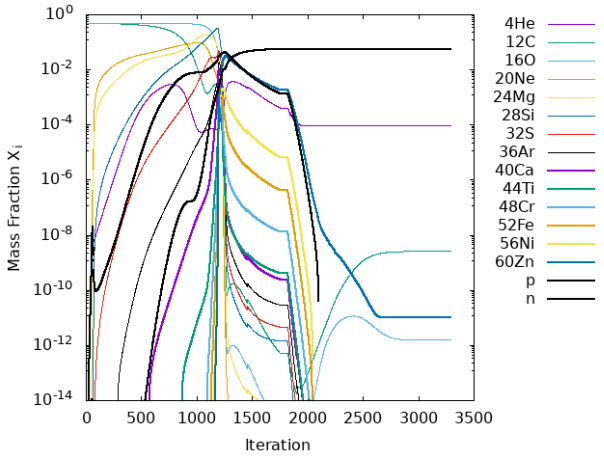

(*c*) *Net87*

Figure 10: Nucleosynthesis evolution comparison for a C+O combustion at initial density $\rho_9 = 2$.

5.2 High Density 49%C+49%O+2%Ne Combustion

In some cases, White Dwarfs present traces of other elements such as Neon. In this section, we wanted to simulate the previous C+O scenario with the addition of some ^{22}Ne to the combustion. This isotope is mainly produced during the He-burning stage of a red-giant and possesses an excess of neutrons though it is a stable nucleus. During the explosion, high temperatures make this nuclei to photodisintegrate releasing its neutron load and altering the outcome of the nucleosynthesis.

The results shown in Table 5 show that the addition of ^{22}Ne into the mixture makes the initial value of the electron molar fraction $Y_e \sim 0.4991$, which is slightly lower than the canonical value 0.5. Thus, the abundances of neutrons and more neutronized isotopes are increased compared to the case of a pure a C+O mixture.

	Net87						Net86					
	$\rho_9 = 2$		$\rho_9 = 1$		$\rho_9 = 0.1$		$\rho_9 = 2$		$\rho_9 = 1$		$\rho_9 = 0.1$	
	NSE	Freeze	NSE	Freeze	NSE	Freeze	NSE	Freeze	NSE	Freeze	NSE	Freeze
T_9	9,4	9,9(-3)	9,3	1,0(-2)	7,3	1,0(-2)	10,1	1,0(-2)	9,4	1,0(-2)	7,1	9,9(-3)
Pr_{27}	1,3	2,5(-9)	6,0(-1)	5,4(-10)	4,6(-2)	3,1(-11)	1,5	1,4(-10)	6,6(-1)	1,1(-10)	4,5(-2)	3,1(-11)
Y_e	0,4565	0,4564	0,4660	0,4653	0,4933	0,4929	0,4991	0,4991	0,4991	0,4991	0,4991	0,4991
^{1}H	1,3(-3)	0	6,0(-3)	0	2,1(-2)	1,1(-14)	4,1(-2)	3,6(-13)	3,9(-2)	4,2(-13)	3,1(-2)	7,5(-13)
n	5,5(-2)	5,4(-2)	4,1(-2)	3,6(-2)	1,7(-3)	0	1,2(-2)	0	9,6(-3)	0	3,3(-4)	0
^{4}He	4,1(-4)	9,3(-5)	7,7(-4)	2,8(-3)	9,2(-4)	1,2(-2)	3,5(-3)	7,5(-3)	1,3(-3)	8,3(-3)	5,3(-4)	1,2(-2)
^{12}C	4,8(-13)	2,4(-9)	8,7(-13)	4,3(-6)	3,6(-13)	1,9(-5)	1,4(-10)	1,0(-5)	3,7(-12)	1,2(-5)	4,8(-12)	1,9(-5)
^{16}O	1,9(-15)	1,5(-12)	2,2(-15)	2,5(-9)	4,0(-15)	1,1(-8)	8,6(-13)	5,9(-9)	1,8(-14)	6,9(-9)	8,4(-13)	1,1(-8)
^{20}Ne	0	0	0	0	0	7,4(-9)	0	3,4(-9)	0	4,1(-9)	1,1(-14)	7,2(-9)
^{21}Ne	0	0	0	0	0	5,0(-8)	0	2,1(-7)	0	1,9(-7)	0	1,2(-7)
^{22}Ne	6,5(E-15)	2,0(E-8)	0	2,4(-4)	0	0	0	0	0	0	0	0
^{21}Na	0	0	0	0	0	0	0	0	0	0	0	0
^{22}Na	0	0	0	0	0	3,6(-14)	0	1,2(-13)	0	1,6(-13)	0	4,3(-13)
^{23}Na	8,6(-15)	3,1(-9)	2,4(-15)	4,0(-7)	0	1,6(-8)	8,5(-15)	3,3(-9)	5,4(-15)	3,6(-9)	1,2(-14)	4,9(-9)
^{22}Mg	0	0	0	0	0	3,0(-11)	0	4,9(-10)	0	5,1(-10)	0	5,9(-10)
^{23}Mg	0	0	0	0	0	0	0	0	0	0	0	0
^{24}Mg	6,7(-15)	0	5,2(-15)	0	5,5(-15)	7,6(-8)	9,7(-14)	3,0(-8)	6,5(-14)	3,7(-8)	1,4(-12)	7,4(-8)
^{25}Mg	0	0	0	0	0	2,3(-8)	2,7(-14)	1,1(-7)	6,2(-15)	9,8(-8)	4,8(-14)	5,9(-8)
^{26}Mg	2,0(-12)	2,0(-10)	2,9(-13)	2,9(-5)	3,2(-15)	0	3,5(-13)	0	1,1(-13)	0	5,3(-14)	0
^{25}Al	0	0	2,7(-15)	0	0	0	6,3(-14)	0	1,6(-14)	0	5,1(-14)	0
^{26}Al	0	0	0	0	0	1,4(-13)	0	4,0(-13)	0	5,4(-13)	3,1(-15)	1,6(-12)
^{27}Al	1,5(-12)	1,1(-11)	5,6(-13)	1,0(-8)	4,4(-14)	1,5(-6)	3,5(-12)	3,1(-7)	1,2(-12)	3,8(-7)	2,3(-12)	7,4(-7)
^{26}Si	0	0	0	0	0	1,7(-11)	0	2,3(-10)	0	2,5(-10)	0	3,3(-10)
^{27}Si	6,4(-14)	0	2,1(-14)	0	0	0	1,2(-13)	0	4,9(-14)	0	1,2(-13)	0
^{28}Si	1,5(-12)	0	1,5(-12)	0	2,7(-12)	4,7(-7)	3,6(-11)	1,9(-7)	1,6(-11)	2,3(-7)	4,2(-10)	4,9(-7)
^{29}Si	3,4(-15)	0	4,2(-15)	0	8,0(-15)	8,3(-10)	1,4(-12)	4,9(-9)	2,9(-13)	4,2(-9)	1,7(-12)	2,4(-9)
^{30}Si	1,0(-9)	3,2(-11)	1,9(-10)	8,1(-5)	6,2(-12)	0	2,2(-10)	0	7,4(-11)	0	8,4(-11)	0
^{29}P	3,0(-13)	0	3,1(-13)	0	1,4(-13)	0	1,5(-11)	0	3,7(-12)	0	1,4(-11)	0
^{30}P	0	0	0	0	3,0(-15)	1,4(-11)	3,5(-13)	4,3(-11)	9,8(-14)	5,1(-11)	8,2(-13)	1,0(-10)
^{31}P	1,2(-10)	4,3(-14)	5,7(-11)	2,1(-10)	1,0(-11)	1,3(-6)	4,1(-10)	2,8(-7)	1,3(-10)	3,4(-7)	3,1(-10)	6,2(-7)
^{30}S	0	0	0	0	0	2,5(-11)	3,7(-15)	2,9(-10)	0	3,2(-10)	4,6(-15)	4,1(-10)
^{31}S	2,6(-11)	0	1,1(-11)	0	1,8(-12)	0	6,9(-11)	0	2,3(-11)	0	9,3(-11)	0
^{32}S	4,9(-12)	0	6,1(-12)	0	1,2(-11)	1,6(-6)	2,0(-10)	6,8(-7)	7,3(-11)	8,6(-7)	8,5(-10)	1,9(-6)
^{33}S	6,6(-15)	0	2,0(-14)	0	3,7(-14)	6,9(-10)	8,3(-12)	3,2(-9)	1,6(-12)	2,8(-9)	3,7(E-12)	1,8(E-9)
^{34}S	1,3(-8)	1,6(-10)	3,2(-9)	4,3(-5)	1,8(-10)	1,4(-13)	4,0(-9)	5,0(-15)	1,4(-9)	5,5(-15)	1,5(E-9)	6,9(-15)
^{33}Cl	1,5(-12)	0	2,0(-12)	0	1,0(-12)	6,0(-15)	1,1(-10)	5,1(-15)	2,7(-11)	4,0(-15)	4,9(-11)	0
^{34}Cl	0	0	6,4(-15)	0	1,2(-14)	1,6(-12)	2,2(-12)	5,5(-12)	4,8(-13)	7,1(-12)	1,6(-12)	2,0(-11)
^{35}Cl	7,9(-10)	1,4(-14)	4,8(-10)	1,3(-11)	1,2(-10)	2,7(-6)	3,9(-9)	5,1(-7)	1,2(-9)	6,4(-7)	2,1(-9)	1,3(-6)
^{34}Ar	0	0	0	0	0	2,6(-11)	2,0(-14)	3,2(-10)	0	3,4(-10)	7,6(-15)	4,4(-10)
^{35}Ar	2,0(-10)	0	1,1(-10)	0	2,2(-11)	0	8,2(-10)	0	2,5(-10)	0	5,2(-10)	0
^{36}Ar	3,0(-11)	0	4,8(-11)	0	1,2(-10)	3,0(-6)	1,6(-9)	1,6(-6)	6,5(-10)	1,9(-6)	5,1(-9)	3,9(E-6)
^{37}Ar	2,8(E-14)	0	1,1(-13)	0	3,1(-13)	3,1(-9)	4,2(-11)	1,1(-8)	9,7(-12)	1,0(-8)	1,9(-11)	7,1(-9)
^{38}Ar	1,4(-7)	3,8(-9)	4,6(-8)	2,0(-5)	4,2(E-9)	2,7(-13)	5,3(-8)	9,6(-15)	2,2(-8)	1,0(-14)	2,4(-8)	1,4(-14)
^{37}K	8,9(E-12)	0	1,5(-11)	0	1,2(-11)	2,7(-13)	8,0(-10)	1,8(-13)	2,3(-10)	1,5(-13)	3,5(-10)	7,8(-14)
^{38}K	9,2(E-15)	0	3,3(-14)	0	6,6(-14)	8,4(-14)	1,2(-11)	4,1(-13)	2,8(-12)	5,7(-13)	4,8(-12)	1,7(-12)
^{39}K	7,1(-9)	3,3(-13)	5,6(-9)	4,7(-12)	2,5(-9)	3,4(-6)	4,1(-8)	6,6(-7)	1,6(-8)	8,2(-7)	3,0(-8)	1,7(-6)
^{38}Ca	0	0	0	0	0	4,1(-12)	8,1(-14)	6,2(-11)	1,4(-14)	6,5(-11)	1,8(-14)	7,4(-11)
^{39}Ca	1,6(-9)	0	1,1(-9)	0	2,8(-10)	0	8,2(-9)	0	2,9(-9)	0	4,1(-9)	0
^{40}Ca	2,5(-10)	0	5,0(-10)	0	2,1(-9)	4,7(-5)	1,7(-8)	2,0(-5)	7,8(-9)	2,5(-5)	6,1(-8)	5,0(E-5)
^{41}Ca	3,6(E-14)	0	1,8(-13)	0	2,9(-13)	2,2(-10)	9,4(-11)	6,9(-10)	1,9(-11)	6,8(-10)	1,0(-11)	6,2(-10)
^{42}Ca	1,2(-6)	2,8(-8)	4,9(-7)	2,7(-5)	4,0(-8)	1,1(-11)	6,7(-7)	3,2(-13)	2,7(-7)	3,4(-13)	1,4(-7)	4,2(-13)
^{41}Sc	2,9(-11)	0	6,0(-11)	0	3,6(-11)	1,0(-11)	4,0(-9)	4,6(-12)	1,1(-9)	4,5(-12)	6,4(-10)	4,1(-12)
^{42}Sc	5,6(-14)	0	2,5(-13)	0	6,6(-13)	0	1,0(-10)	0	2,5(-11)	1,0(-14)	3,1(-11)	2,6(-14)
^{43}Sc	3,3(-8)	8,8(-15)	3,1(-8)	3,7(-13)	8,0(-9)	1,3(-8)	3,0(-7)	1,9(-9)	1,0(-7)	2,1(-9)	5,6(-8)	2,9(-9)
^{42}Ti	0	0	0	0	0	0	3,3(-13)	2,0(-14)	5,3(-14)	1,8(-14)	2,8(-14)	1,4(-14)
^{43}Ti	1,5(-8)	0	1,3(-8)	0	5,0(-9)	9,8(-11)	1,0(-7)	1,2(-11)	3,9(-8)	1,2(-11)	4,7(-8)	1,1(-11)
^{44}Ti	4,1(-10)	0	1,1(-9)	0	2,6(-9)	2,7(-5)	2,3(-8)	1,2(-5)	1,8(-8)	1,4(-5)	4,1(-8)	2,8(-5)
^{45}Ti	7,0(-13)	0	4,6(-12)	0	1,1(-11)	8,9(-8)	1,2(-9)	1,6(-7)	5,3(-10)	1,6(E-7)	2,5(-10)	1,5(-7)
^{46}Ti	2,8(-5)	1,8(-6)	1,5(-5)	1,3(-5)	3,1(-6)	1,0(-10)	8,9(-6)	2,9(-12)	9,1(-6)	3,2(-12)	7,5(-6)	4,9(-12)
^{45}V	3,1(-10)	0	8,5(-10)	0	8,1(-10)	6,1(-10)	2,8(-8)	2,1(-10)	1,6(-8)	2,0(-10)	9,2(-9)	1,7(-10)
^{46}V	1,2(-13)	0	7,1(-13)	0	2,0(-12)	1,6(-13)	1,4(-10)	7,5(-13)	7,5(-11)	1,0(-12)	5,3(E-11)	2,6(-12)
^{47}V	9,2(-7)	2,3(-12)	1,2(-6)	2,4(-13)	7,5(-7)	4,9(-7)	5,0(-6)	7,1(-8)	4,2(-6)	8,4(-8)	3,6(-6)	1,5(-7)
^{46}Cr	0	0	0	0	0	1,0(-10)	7,4(-13)	1,5(-9)	2,3(-13)	1,6(-9)	9,3(-14)	1,9(-9)
^{47}Cr	1,1(-7)	0	1,2(-7)	0	5,5(-8)	3,2(-11)	5,0(-7)	2,1(-12)	4,0(-7)	1,9(-12)	3,0(-7)	1,4(-12)
^{48}Cr	1,3(-8)	0	4,3(-8)	0	2,0(-7)	8,1(-5)	9,9(-7)	3,6(-5)	8,5(-7)	4,3(-5)	2,3(-6)	8,6(-5)
^{49}Cr	2,5(-11)	0	2,0(-10)	0	1,3(-9)	5,2(-7)	5,2(-8)	6,7(-7)	2,7(-8)	6,9(-7)	2,1(-8)	7,3(-7)
^{50}Cr	2,8(-3)	6,6(-4)	1,9(-3)	1,7(-5)	8,8(-4)	3,9(-11)	1,2(-3)	1,1(-12)	1,3(-3)	1,2(-12)	1,6(-3)	1,7(-12)
^{49}Mn	1,6(-8)	0	5,4(-8)	0	1,2(-7)	6,7(-9)	1,9(-6)	1,5(-9)	1,2(-6)	1,5(-9)	9,6(-7)	1,4(-9)
^{50}Mn	4,3(-12)	0	3,2(E-11)	0	1,7(-10)	1,7(-11)	7,0(-9)	8,0(-11)	3,9(-9)	8,6(-11)	3,3(-9)	1,3(-10)
^{51}Mn	5,0(-5)	8,9(-10)	8,2(-5)	1,9(-13)	1,3(-4)	1,6(-7)	3,6(-4)	2,5(-8)	3,3(-4)	2,8(-8)	4,5(-4)	4,6(-8)
^{50}Fe	0	0	2,3(-14)	0	1,4(-13)	3,9(-11)	5,7(-11)	5,6(-10)	1,7(-11)	5,8(-10)	5,1(-12)	6,3(-10)
^{51}Fe	6,1(-6)	0	9,0(-6)	0	9,8(-6)	4,6(-9)	3,8(-5)	2,2(-10)	3,4(-5)	2,1(-10)	4,1(-5)	1,9(-10)
^{52}Fe	4,2(-7)	0	1,7(-6)	0	1,6(-5)	1,5(-4)	4,4(-5)	8,6(-5)	3,9(-5)	1,0(-4)	1,3(-4)	1,8(E-4)
^{53}Fe	3,8(-10)	0	3,8(-9)	0	4,3(-8)	1,9(-6)	1,1(-6)	2,3(-6)	6,0(-7)	2,4(-6)	4,9(-7)	2,7(-6)
^{54}Fe	1,4(-1)	1,1(-1)	1,2(-1)	1,0(-2)	1,1(-1)	1,1(-9)	8,1(-2)	5,8(-11)	9,2(-2)	5,0(-11)	1,4(-1)	3,2(-11)
^{53}Co	4,3(-7)	0	1,9(-6)	0	7,5(-6)	2,6(-7)	7,5(-5)	5,7(-8)	4,9(-5)	5,6(-8)	4,4(-5)	5,5(-8)
^{54}Co	5,1(-11)	0	4,6(-10)	0	4,2(-9)	3,1(-13)	1,3(-7)	2,2(-12)	6,7(-8)	2,3(-12)	5,8(-8)	3,4(-12)
^{55}Co	1,4(-3)	5,5(-8)	2,8(-3)	3,9(-11)	9,7(-3)	8,8(-7)	1,3(-2)	2,4(-7)	1,3(-2)	2,2(-7)	2,6(-2)	1,6(-7)
^{54}Ni	8,3(-15)	0	1,8(-13)	0	2,0(-12)	5,0(-13)	5,0(-10)	1,2(-11)	1,6(-10)	1,1(-11)	5,1(-11)	9,1(-12)
^{55}Ni	2,6(-4)	0	4,8(-4)	0	9,4(-4)	4,1(-7)	2,3(-3)	1,9(-8)	2,1(-3)	2,0(-8)	2,9(-3)	2,3(-8)

	Net87						Net86					
	$\rho_9 = 2$		$\rho_9 = 1$		$\rho_9 = 0.1$		$\rho_9 = 2$		$\rho_9 = 1$		$\rho_9 = 0.1$	
	NSE	Freeze	NSE	Freeze	NSE	Freeze	NSE	Freeze	NSE	Freeze	NSE	Freeze
^{56}Ni	6,5(-6)	0	3,2(-5)	0	6,7(-4)	4,1(-1)	9,2(-4)	6,6(-1)	8,8(-4)	6,6(-1)	4,0(-3)	6,8(-1)
^{57}Ni	3,3(E-10)	0	3,8(-9)	0	1,6(-8)	5,0(-10)	2,2(-6)	1,6(-8)	7,5(-7)	1,3(-8)	1,1(-7)	5,9(-9)
^{58}Ni	8,0(-1)	8,4(-1)	8,2(-1)	9,5(-1)	8,3(-1)	3,8(-1)	7,7(-1)	2,8(-2)	7,8(-1)	2,9(-2)	7,3(-1)	3,0(-2)
^{57}Cu	1,6(-6)	0	8,4(-6)	0	2,8(-5)	4,3(-6)	4,9(-4)	2,2(-5)	2,7(-4)	1,9(-5)	1,1(-4)	1,2(-5)
^{58}Cu	5,8(-10)	0	6,4(-9)	0	6,6(-8)	2,7(-14)	2,4(-6)	2,5(-12)	1,1(-6)	2,6(-12)	6,2(-7)	2,8(-12)
^{59}Cu	1,8(-3)	1,1(-11)	4,3(-3)	5,7(-12)	6,3(-3)	7,5(-3)	3,7(-2)	2,9(-3)	2,5(-2)	2,8(-3)	1,0(-2)	2,3(-3)
^{58}Zn	2,3(-14)	0	5,6(-13)	0	4,6(-12)	0	2,4(-9)	0	6,1(-10)	0	7,4(-11)	0
^{59}Zn	3,0(-3)	0	6,7(-3)	0	2,3(E-2)	5,9(-2)	3,7(-2)	4,5(E-2)	3,4(-2)	4,5(-2)	4,9(-2)	4,3(E-2)
^{60}Zn	1,3(-6)	0	7,4(-6)	0	3,3(-5)	1,3(-1)	4,3(-4)	2,6(-1)	2,6(-4)	2,5(-1)	1,1(-4)	2,3(-1)

Table 5: Net86 and Net87 nucleosynthesis yields after combustion of a mixture of $49\%C+49\%O+2\%^{22}Ne$ *at* $\rho_9 = 2, 1, 0.1$*, before the adiabatic expansion* (NSE) *and after the expansion* $(Freeze\text{-}out)$*.*

5.3 Low Density He Combustion

A completely different case is the explosive burning of helium taking place at the outermost layers of accreting White Dwarfs. The He transferred from the companion star is accumulated instead of burned and eventually ignites propagating the detonation wave and igniting the core. This is the so-called double detonation scenario. This problem needs a multi-dimensional hydrodynamical approach because the ignition of the helium in the shell might take place in either a single point or few points of the layer.

In this regime, the densities are significantly lower than that of the core, taking values between $\rho_6 = 2$ to $\rho_6 = 0.5$ and the maximum temperatures achieved are of the order of 3 and 4 billion Kelvins. In these relatively softer conditions electron captures do not play significant role, for this reason only a comparison between Net14 and Net86 has been studied.

5.3.1 Temperature, Pressure and Released Energy

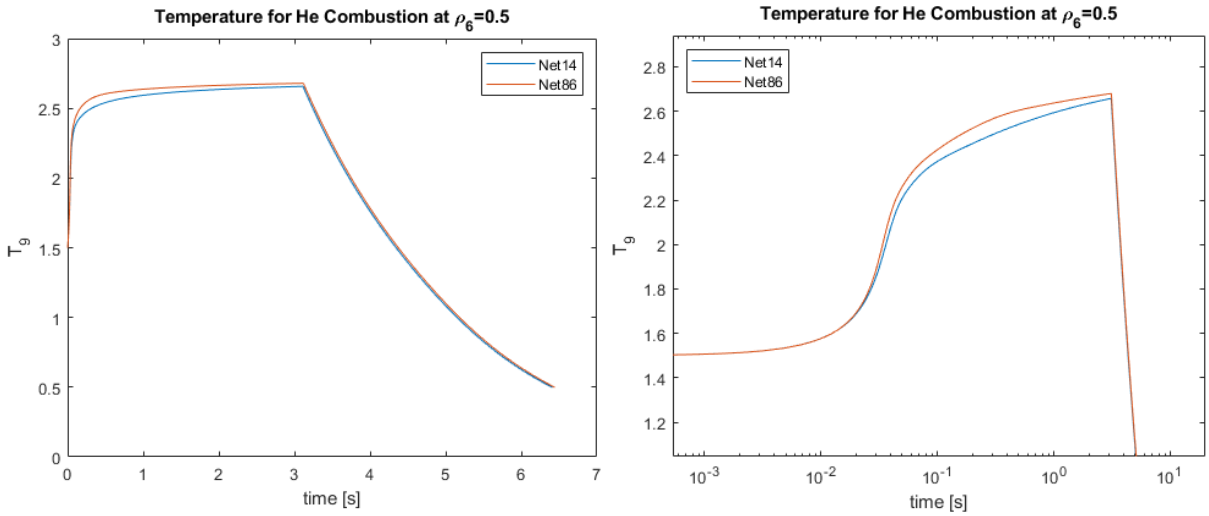

Figure 11: Temperature evolution comparison for a He combustion at $\rho_6 = 0.5$*, both in linear* $(left)$ *and logarithmic* $(right)$ *time-scale.*

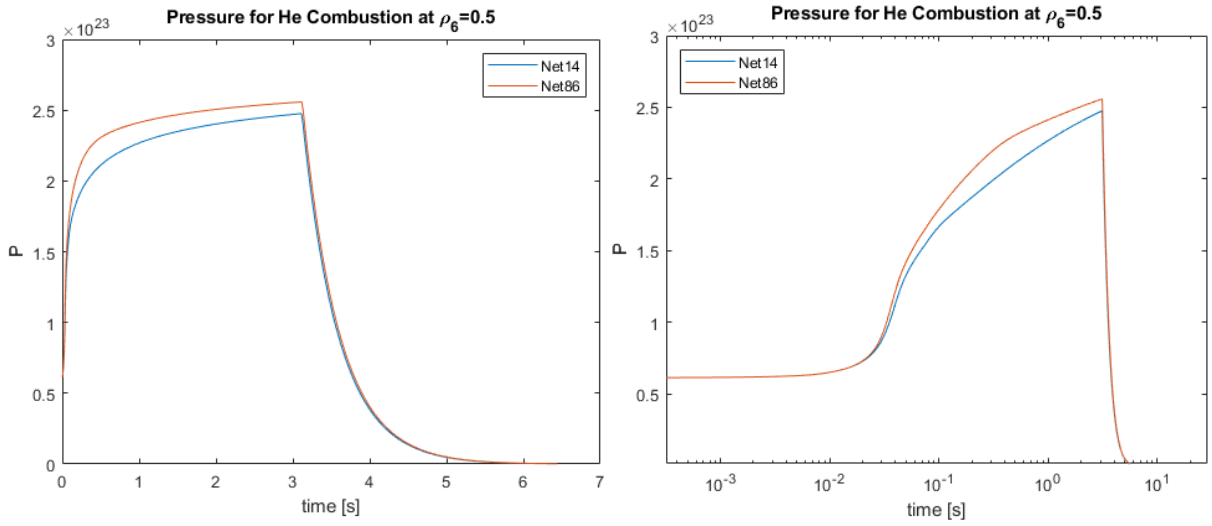

Figure 12: Same as figure 11 but for the pressure.

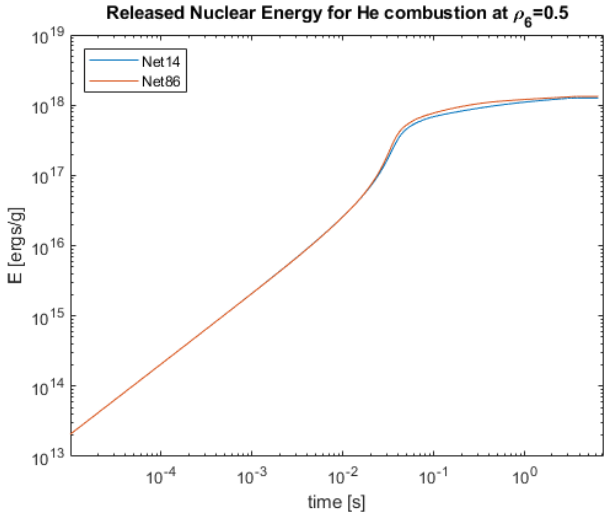

Figure 13: Same as figure 11 and 12 but for the released nuclear energy.

5.3.2 Nucleosynthesis Yields of He Combustion

	Net86				Net14			
	$\rho_6 = 2$		$\rho_6 = 0.5$		$\rho_6 = 2$		$\rho_6 = 0.5$	
	NSE	Freeze	NSE	Freeze	NSE	Freeze	NSE	Freeze
T_9	3,6	9,9(-3)	2,6	9,9(-3)	3,7	9,9(-3)	2,6	1,0(-2)
Pr_{27}	1,0(-3)	3,4(-13)	2,4(-4)	2,4(-13)	1,1(-3)	3,9(-13)	2,3(-4)	2,2(-13)
Y_e	0,5000	0,5000	0,5000	0,5000	0,5000	0,5000	0,5000	0,5000
^1He	1,2(-2)	4,9(-6)	2,0(-3)	6,8(-6)				
n	1,2(-11)	0	0	0				
^4He	5,6(-2)	6,2(-2)	1,0(-1)	9,7(-2)	4,0(E-2)	3,9(E-2)	1,2(E-1)	1,1(E-1)
^{12}C	5,9(-7)	5,0(-5)	1,1(-5)	1,3(-4)	2,6(E-7)	1,5(E-5)	1,7(E-5)	2,0(E-4)
^{16}O	4,6(-8)	2,9(-8)	1,6(-7)	7,9(-8)	2,5(E-8)	8,5(E-9)	2,2(E-7)	1,2(E-7)
^{20}Ne	9,6(-11)	4,6(-10)	4,3(-9)	6,6(-10)	6,6(E-10)	4,7(E-9)	1,3(E-8)	8,1(E-8)
^{21}Ne	7,6(-7)	7,6(-7)	4,1(-9)	4,2(-9)				
^{22}Ne	0	0	0	0				
^{21}Na	1,6(-10)	0	0	0				
^{22}Na	2,9(-13)	5,9(-10)	1,2(-11)	9,4(-10)				
^{23}Na	1,1(-10)	0	2,8(-9)	0				
^{22}Mg	4,9(-13)	1,3(-5)	1,0(-9)	7,9(-7)				
^{23}Mg	2,3(-13)	0	0	0				
^{24}Mg	7,0(-11)	1,3(-9)	2,3(-9)	1,0(-9)	2,7(E-9)	4,9(E-8)	6,7(E-8)	9,6(E-7)
^{25}Mg	2,9(-7)	2,9(-7)	2,2(-9)	2,2(-9)				

	Net86				Net14			
	$\rho_6 = 2$		$\rho_6 = 0.5$		$\rho_6 = 2$		$\rho_6 = 0.5$	
	NSE	Freeze	NSE	Freeze	NSE	Freeze	NSE	Freeze
^{26}Mg	0	0	0	0				
^{25}Al	1,3(-10)	0	0	0				
^{26}Al	1,3(-13)	2,4(-9)	3,8(-12)	2,1(-9)				
^{27}Al	1,1(-10)	9,0(-13)	5,2(-9)	2,1(-13)				
^{26}Si	2,0(-13)	5,4(-6)	3,1(-10)	8,4(-7)				
^{27}Si	5,1(-13)	0	0	0				
^{28}Si	6,6(-10)	4,2(-10)	3,2(-8)	3,4(-10)	1,3(E-8)	4,6(E-7)	4,9(E-7)	8,9(E-6)
^{29}Si	3,0(-10)	8,8(-10)	1,5(-10)	1,6(-10)				
^{30}Si	4,9(-14)	0	0	0				
^{29}P	7,1(-12)	0	4,0(-14)	0				
^{30}P	1,8(-12)	1,7(-9)	1,4(-10)	2,5(-9)				
^{31}P	2,9(-10)	3,5(-13)	1,5(-8)	1,3(-12)				
^{30}S	2,4(-13)	9,8(-6)	2,8(-10)	1,2(-5)				
^{31}S	3,5(-13)	0	0	0				
^{32}S	2,1(-9)	6,9(-10)	1,3(-7)	2,4(-6)	9,1(E-8)	4,9(E-6)	4,4(E-6)	9,2(E-5)
^{33}S	1,8(-10)	9,9(-10)	9,5(-11)	9,6(-11)				
^{34}S	5,9(-13)	0	0	0				
^{33}Cl	8,9(-12)	0	5,6(-14)	0				
^{34}Cl	2,7(-12)	6,3(-10)	1,5(-10)	3,3(-6)				
^{35}Cl	3,5(-10)	7,9(-14)	2,0(-8)	2,5(-10)				
^{34}Ar	4,1(-13)	5,3(-6)	4,6(-10)	1,1(-5)				
^{35}Ar	2,0(-12)	0	0	0				
^{36}Ar	8,5(-9)	1,5(-7)	7,4(-7)	3,7(-5)	2,1(E-6)	5,1(E-5)	1,8(E-4)	8,9(E-4)
^{37}Ar	6,9(-10)	4,6(-9)	4,5(-10)	4,5(-10)				
^{38}Ar	1,1(-12)	0	0	0				
^{37}K	6,7(-11)	0	7,5(-13)	0				
^{38}K	2,7(-12)	1,5(-8)	1,3(-10)	5,4(-6)				
^{39}K	6,8(-10)	2,1(-11)	4,4(-8)	7,4(-9)				
^{38}Ca	2,9(-13)	2,7(-6)	2,3(-10)	1,6(-6)				
^{39}Ca	1,2(-11)	0	8,8(-15)	0				
^{40}Ca	1,7(-7)	1,3(-4)	3,0(-5)	5,2(-4)	1,6(E-4)	2,2(E-5)	1,2(E-3)	5,3(E-4)
^{41}Ca	7,5(-12)	1,2(-9)	2,6(-9)	3,0(-9)				
^{42}Ca	2,9(-11)	0	0	0				
^{41}Sc	8,6(-12)	0	1,2(-10)	0				
^{42}Sc	9,1(-12)	2,9(-8)	3,5(-10)	1,6(-7)				
^{43}Sc	5,1(-10)	5,0(-14)	1,1(-8)	7,7(-13)				
^{42}Ti	4,1(-14)	1,0(-7)	1,0(-11)	5,3(-9)				
^{43}Ti	1,1(-10)	0	3,0(-10)	0				
^{44}Ti	8,2(-8)	3,0(-5)	2,6(-5)	2,7(-4)	9,5(E-5)	6,4(E-4)	5,7(E-1)	5,7(E-1)
^{45}Ti	7,6(-9)	1,5(-7)	5,8(-8)	5,9(-8)				
^{46}Ti	4,4(-11)	0	0	0				
^{45}V	3,2(-9)	0	1,1(-9)	0				
^{46}V	4,6(-11)	7,0(-7)	5,9(-9)	9,0(-6)				
^{47}V	1,8(-9)	5,5(-11)	6,4(-8)	3,8(-9)				
^{46}Cr	3,3(-12)	5,3(-5)	1,0(-8)	1,1(-6)				
^{47}Cr	4,3(-9)	0	5,6(-11)	0				
^{48}Cr	2,2(-7)	2,8(-5)	2,0(-4)	7,7(-4)	8,4(E-4)	1,0(E-3)	3,0(E-1)	3,1(E-1)
^{49}Cr	4,7(-8)	7,5(-7)	7,8(-7)	8,0(-7)				
^{50}Cr	1,7(-10)	0	1,4(-10)	0				
^{49}Mn	3,1(-8)	7,3(-15)	2,1(-8)	3,1(-13)				
^{50}Mn	2,4(-10)	1,5(-6)	1,0(-10)	4,9(-5)				
^{51}Mn	5,3(-9)	6,4(-12)	1,1(-7)	3,5(-9)				
^{50}Fe	3,2(-12)	2,1(-4)	4,5(-8)	1,1(-5)				
^{51}Fe	7,6(-8)	0	4,1(-9)	0				
^{52}Fe	1,1(-6)	3,9(-4)	1,5(-3)	1,8(-3)	6,8(E-3)	6,2(E-3)	6,9(E-3)	7,2(E-3)
^{53}Fe	1,4(-7)	3,6(-6)	1,1(-6)	1,3(-6)				
^{54}Fe	1,3(-4)	0	3,4(-8)	0				
^{53}Co	2,9(-7)	2,1(-12)	1,2(-7)	1,5(-10)				
^{54}Co	2,3(-10)	4,1(-7)	1,3(-10)	2,4(-6)				
^{55}Co	2,2(-3)	6,5(-11)	9,7(-6)	2,3(-8)				
^{54}Ni	1,4(-12)	6,5(-6)	1,1(-8)	8,7(-8)				
^{55}Ni	1,2(-6)	0	5,7(-8)	4,8(-12)				
^{56}Ni	5,2(-1)	6,9(-1)	6,6(-1)	6,3(-1)	9,5(E-1)	9,5(E-1)	2,7(E-5)	2,9(E-5)
^{57}Ni	3,6(-7)	2,0(-2)	4,8(-11)	4,0(-8)				
^{58}Ni	3,1(-1)	5,3(-10)	5,4(-2)	5,7(-5)				
^{57}Cu	1,8(-4)	1,3(-2)	1,1(-8)	2,5(-7)				
^{58}Cu	3,9(-6)	1,3(-6)	7,3(-7)	1,4(-6)				
^{59}Cu	1,6(-2)	1,7(-7)	9,8(-3)	5,0(-4)				
^{58}Zn	2,9(-10)	2,6(-10)	5,1(-11)	1,6(-10)				
^{59}Zn	7,6(-2)	2,0(-2)	2,8(-6)	2,6(-6)				
^{60}Zn	1,0(-2)	1,9	1,7(-1)	2,7(-1)	2,8(E-4)	3,3(E-3)	2,4(E-7)	3,0(E-7)

Table 6: Net86 and Net14 Nucleosynthesis yields of He-burning for $\rho_6 = 2, 0.5$, before the adiabatic expansion (NSE) and after the expansion (Freeze-out).

The main difference in the results shown in table 6 is the discrepancy in the heavy nuclei abundances, especially the metallic elements and for the lowest density. For example, the synthesis of ^{60}Zn is seriously limited when using Net14 in comparison with Net86, as well as the production of ^{56}Ni for $\rho_6 = 0.5$. The alpha reactions turn out to be halted at low densities and the reactions can not continue beyond ^{44}Ti and ^{48}Cr in Net14, whereas in Net86 other paths to synthesis of heavier isotopes are still possible.

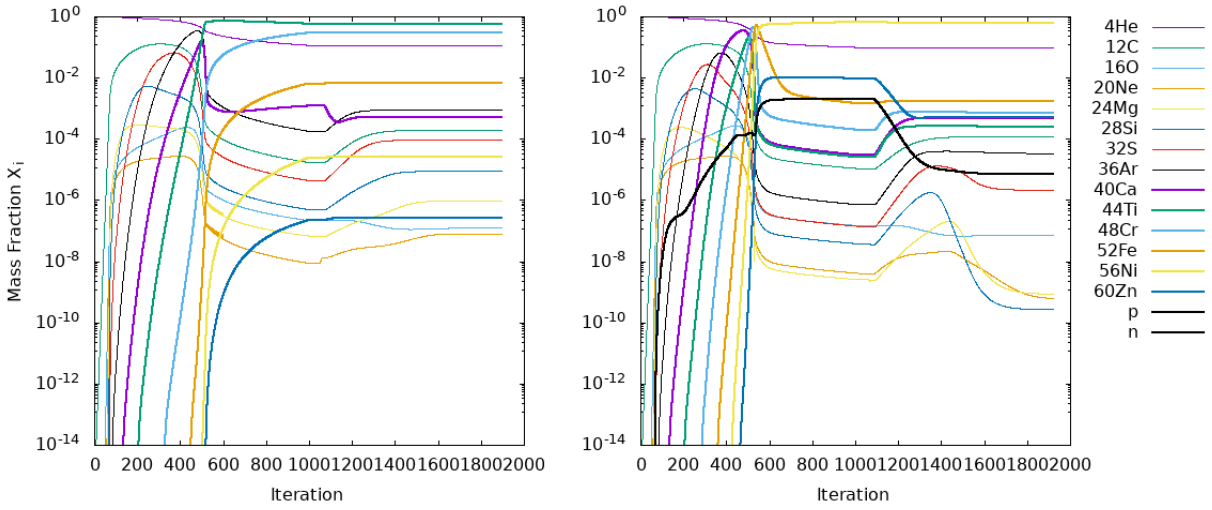

Figure 14: Nucleosynthesis evolution comparison for a He combustion at initial density $\rho_6 = 0.5$, for Net14 (Left) and Net86 (Right).

The evolutions shown in Figure 14 may help to visualize this effect: the rate of ^{56}Ni is so low in Net14 that can not produce as much as in Net86 before the adiabatic expansion takes place and the elements that remain the most dominant are lighter metals as ^{44}Ti and ^{48}Cr. However, the thermodynamical evolution provided for both nuclear networks (shown in 11, 12 and 13) are very similar, so the cause of this discrepancies is in fact the architecture of the nets (i.e. the number of different isotopes and their possible nuclear reactions).

This results imply that a small net like Net14 based on alpha captures in not suitable at all for explosive combustion regime at low densities, meaning that the provided yields of the simulations are really bad approximations to those of the real events it aims to replicate.

5.4 Silicon Combustion

Although the aim of this work was to develop Net87 for its use in SN Ia simulations, the model is suitable for performing several different type of tests. One of them is the silicon combustion. Silicon burning is the last possible step on main-sequence stars and, after that, no further fusion takes place, the star collapses and it explodes violently. This is the so-called Type II supernova. The silicon combustion is an endoenergetic process, due to the major role of photodisintegrations, and is performed under nearly isothermal conditions due to the large thermal electron conductivity. In order to maintain the temperature constant the value of the specific heat, which is normally provided by the EOS, was artificially increased so that $\Delta T \sim 0$. We performed this test in both Net14 and Net87 and compared the differences in the nucleosynthesis and the energy generation rate, for a combustion at $\rho_9 = 0.01$ and $T_9 = 6$.

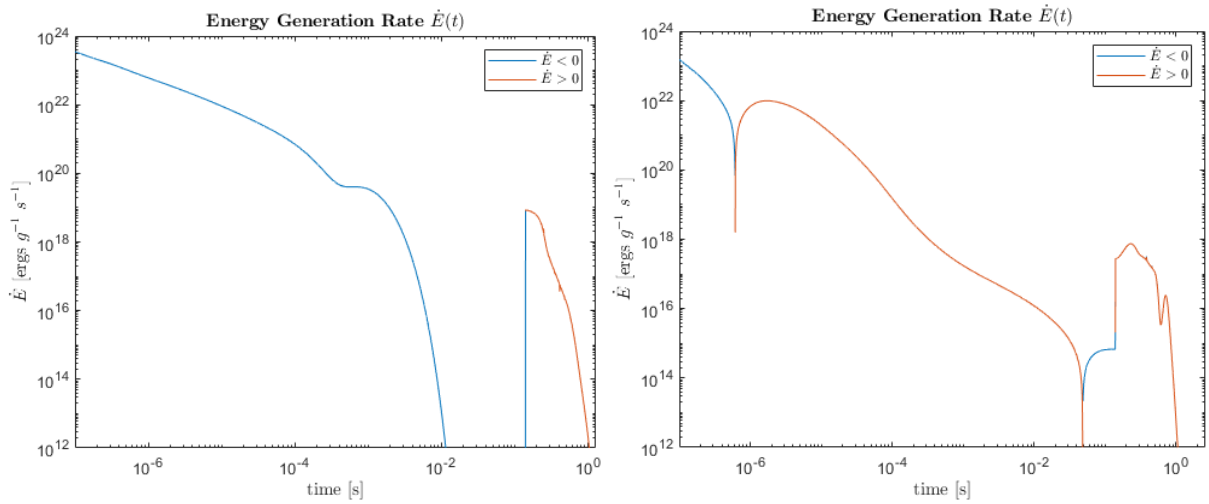

Figure 15: Absolute value of the energy generation rate $\dot{E}$. Absorption of energy in blue and energy release in orange. Net14 (left) and Net87 (right) .

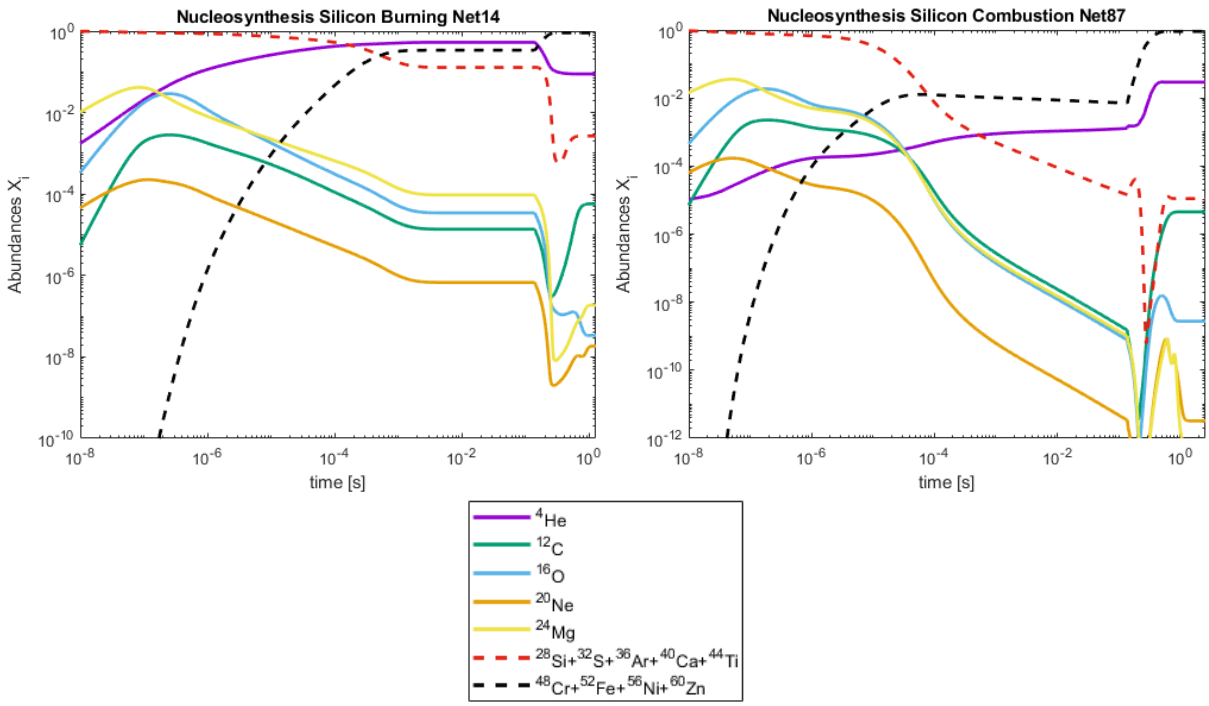

Figure 16: Nucleosynthesis comparison during a silicon Combustion of Net14 (left) and Net87 (Right).

As we can see in Figure 15 the general trend of the released energy is badly represented by Net14. Photodisintegrations take over in a large section of the diagram while exoenergetic direct reactions are only relevant during the adiabatic expansion of the mixture. Net87 shows a much richer structure, showing an alternation in endoenergetic/exoenergetic episodes. Such behaviour is also seen in Figure 16 during the evolution of the abundances. While the abundance of helium is kept high from the very beginning in Net14 it remains quite low in Net87. On another note, during the adiabatic expansion the helium content diminishes in Net14 but it

rises in Net 87. The reduced network overestimates the abundance of intermediate elements at the freezing point. Curiously, both nets lead to a similar amount of high-mass elements after the freezing.

6 Impact on Type Ia supernovae

Once the results of explosive combustion, as a function of the initial fuel composition and density, have been analyzed we can sketch several consequences to the explosion of a real white dwarf. However, the correct depiction of the explosion would need to run a hydrodynamic multi-D code to simulate the event. This task is under way, and we expect to start simulating SN Ia explosions soon, taking advantage of the implementation and checking of Net87 carried out in this project.

6.1 Expected impact in Chandrasekhar-mass models.

Historically, the explosion of a WD with a mass close to the Chandrasekhar-mass limit was considered the standard model of SN Ia explosions. Spherically symmetric models of the explosion led to a notable match with the main observables: light curve, chemical composition of the ejecta shown in the spectra, expanding velocities, etc. Nevertheless, all these hydrodynamical codes shared the weakness of having several adjustable free parameters to artificially fit the observational data. Since the beginning of this century different groups worldwide are running multi-dimensional simulations trying to reproduce the observations from first principles, without introducing ad-hoc free parameters.

A key piece of the simulations is the nuclear network. In this sense, our Net87 is a step forward because it is capable to estimate the nuclear energy input rate with a larger accuracy than a reduced network (as Net14, for example) does. This is a necessary condition to trust the global energetics of the explosion (for example the kinetic energy).

An important point, and a novelty of this work, is that electron captures on protons have been incorporated to this moderately-size network. In the Chandrasekhar-mass models the density of the core is large enough to facilitate a good rate of captures. From the dynamical point of view, the reduction in the number of electrons depressurizes the plasma which provokes a slower expansion rate at the beginning of the explosion changing a bit the path of the event. From our results, it is expected a 10-30% reduction in pressure at $\rho_9 \sim 2$ (See Figure 8).

Each electron capture produces a neutrino which freely escapes from the system. According to early spherically symmetric simulations (i.e. [11]) the neutrino luminosity could be large enough as to be observed, provided that the explosion takes place in the Milky Way. It could be very interesting to study such neutrino signal in multi-D simulations.

Finally, Net87 includes a sufficient number of nuclei as to generate reliable nuclosynthetic yields without the concurrence of further postprocessing with a much larger network. Nevertheless, using some kind of post-processing is unavoidable if we are interested in fine nucleosynthetic details.

6.2 Dominant Nucleus Distribution

White Dwarfs present large variations in density along its distance to the center of the star and during the explosion these differences leave their imprint in the final nucleosynthesis. As shown

in the previous section, high-density combustion produces heavier species than at lower densities. Thus, we can roughly obtain the radial distribution of the more important isotope assuming that the white dwarf suddenly detonates so that the material is burned "in place", without undergoing a previous pre-expansion.

Several combustions performed with Net87 for many different densities provide a relation between the most abundant isotope and the value of density itself. Considering a typical WD with a central density $\rho_9 = 2$ (Total mass around $1.356 M_\odot$) and its density profile $\rho(r)$ (See the red line in Figure 17) given by the construction of the star and superposing this information with the related dominant nucleus, the following figure is obtained:

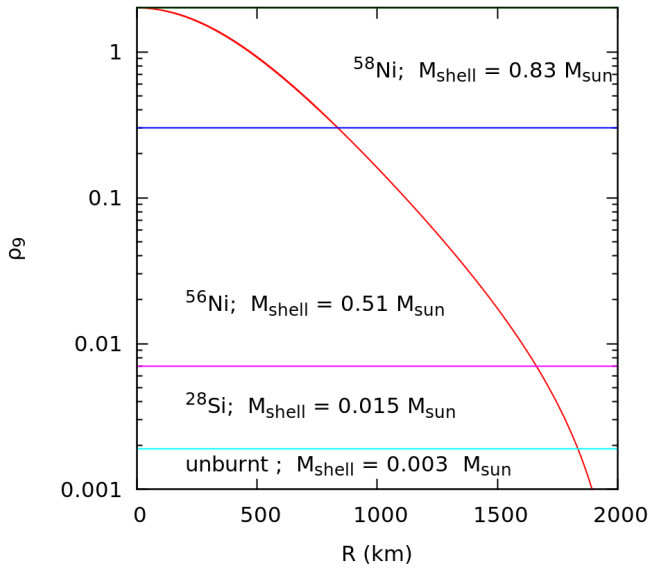

Figure 17: Distribution of the most abundant nuclei after detonation of a M=1.356$M_\odot$ white dwarf

Figure 17 shows the dominance of very specific isotopes after the explosion. The first two interior shells, which actually comprehend roughly 98.67% of the White Dwarf mass, are completely ruled by nickel. The higher densities at the core produce more electron captures and shift the dominance to the more neutronized isotope ^{58}Ni, while in the more intermediate region the most abundant nucleus is ^{56}Ni.The ^{58}Ni is a stable nuclei but ^{56}Ni is radioactive and its disintegration feeds the light curve of the event. Therefore, including e-captures is crucial to understand the peculiarities of the light curve of Type Ia supernova explosions. The third interval corresponds to the shell situated at a distance around 1750 km from the center and is mainly comprised of ^{28}Si; the fourth and outermost shell of the WD remains unburnt, i.e. the fuel has not been exhausted due to the low density.

This results are coherent with those of more sophisticated models, very similar to the so called "pure detonation" models. However, this model is dismissed since it produces too many neutronized elements and little silicon, which is necessary to be abundant to match spectrum observations. Nonetheless, it is really interesting that we reach the same conclusion without the need to run a complete hydrodynamical model.

6.3 Impact on SubChandrasekhar-mass models

Using and extended network of moderate size could also be important to model the so called SubChandrasekhar-mass models of the explosion. These models consist of a core made of carbon and oxygen weighting $\sim$ 0.7-1.0$M_\odot$ surrounded by a tiny shell of helium (mass $\sim 0.03 M_\odot$). At some point the helium is ignited at the base of the He-layer and the ignition propagates all the way through it, which totally evaporates the layer. This combustion of the He-layer induces an over-pressure on the core of the WD, eventually leading to the detonation of the carbon. Such inner carbon detonation consumes the core producing a very energetic display. This model is currently in great interest because it is able not only to reproduce the main SN Ia observables, but also it can account for the observed diversity of SN Ia events. Nevertheless, this scenario requires a multi-D approach to be adequately studied.

One important issue in this models is how to detonate a low density layer made of helium. The 3-α reaction is very dependent on density and very reduced nuclear nets often have difficulties to blow-up the He-layer. As Net87 incorporates additional proton and neutron channels to support the combustion we expect a much better performance of this net to handle with this scenario. Also note that even though electron captures do not play a role during the detonation of the shell (due to the low densities) they can be active once carbon is detonated later at the core where densities are larger than $\rho = 10^7$ g/cm3.

6.4 Expected Impact on Luminosity and the Spectra

Another interesting topic is how the inclusion of electron captures in Net87 gives different nucleosynthesis yields and how will be the impact of this on the luminosity curve and on the characteristic spectra.

As mentioned in the introductory section of this work, the luminosity curve of SN Ia explosions is fed by the decay of ^{56}Ni which makes the decrease of luminosity more gradual along time. The addition of e-captures increases the neutronization of the system and makes the traditional dominance of ^{56}Ni to shift to its more neutronized isotope ^{58}Ni, which is not a radioactive nuclei anymore. In consequence, the material ejected after the explosion is mainly comprised of ^{58}Ni, and thus the luminosity is presumably going to decrease at a faster pace due to the lack of the source of photons from the disintegration of ^{56}Ni.

Although the impact of the ^{56}Ni/^{58}Ni relation on the luminosity curve is a well-known topic, specially in uni-dimensional simulations, our Net87 will help to better understand the effect of that relation regarding the light curve in 3-dimensional simulations.

Conclusions

The implementation of our moderate-size nuclear network Net87 has been totally successful. The original Net86 was upgraded with the addition of an iterative Newton-Raphson solver as well as with the extension to second order semi-implicit integration. Also, the inclusion of the new electron capture reaction needed the tracking of electrons as whole new specie, for that the change of the network name from Net86 to Net87.

The addition of Newton-Raphson has allowed to greatly increase the length of the time-steps taken in the simulations without compromising the accuracy of the results. Thus, more efficient and faster multi-D SN Ia simulations could be possible and we plan to start very soon with the

tests in the full hydrodynamical code SPHYNX [5].

Apart from these implementations and these results, other features were studied to be added but were in the end discarded due to not being technically feasible or worthy. An example for this are the use of linear extrapolations to start the iterative solving process with an initial guess much closer to the solution, which was dismissed due to the increased computational burden. Another example for this is the use of adjusted formulas for the final NSE temperature as a function of the initial composition. This was initially intended to be used to gradually change the implicit parameter from $\theta = 0.5$ to $\theta = 1$ as the combustion approached the NSE regime in order to assure stability, but this was finally not needed since $\theta = 0.5$ already provided good and stable results.

The results provided by the net87 have shown the importance of e-captures since they cause a pressure and temperature reduction as well as an increase in the abundance of more neutronized isotopes. Also, an interesting result was the different nucleosynthesis between Net87 and Net14 in low-density tests, which we interpreted as a lack of reliability from Net14 to be used in this scenarios. Regarding the energies released by the nets, it is quite astonishing the great reduction of released energy provided by Net87 due to the combination of neutrino energy losses and more neutron-rich nucleosynthesis yields.

Personal Thoughts

Well, as this is technically outside of the work, I'm going to allow myself to lower the register to express my thoughts about the project.

What a trip. I mean, What–a–trip, seriously. In the first weeks of the work I was so disoriented that I couldn't find the way to start. Here I have to really thank the aid of both Domingo and Rubén, since they have carried me forward whenever I got stuck and have had the patience to answer my (almost daily) mails having loads of questions. Every 15 days we met in our 16:9 screens and I explained the progress of the work, sometimes with a lot to say and other times with not so much about it.

Also, I have developed the final work of this degree during a fu***** global pandemic, seriously what the hell is that, apart from depressing I mean. Hell, were our now daily meet sessions even a thing before 2020? Ah yes, I still can remember the chaos the day Google services stopped working worldwide, crazy how things have changed this two last years right? Hey you, future-myself, I don't know if you are reading this to remember the good ol' days or something like that, but yeah, I hope you are fine, and wash your hands please!

Anyway, I'm very happy with this project since, for the first time in all these 4 years in the degree, I felt like I was doing something relevant, not any meaningless experiment in a lab or a typical didactic problem of a subject. I knew that the work I was doing was going to be useful in present day studies, this is the real deal you know.

Well I don't want to gabble so much, If you are still here, thank you. Thank you for taking your time to read this work and I really hope you enjoyed it!

Bibliografia

[1] W. D. Arnett. A Possible Model of Supernovae: Detonation of ^{12}C. , 5(2):180–212, Oct. 1969. doi:10.1007/BF00650291.

[2] W. D. Arnett and J. W. Truran. Carbon-Burning Nucleosynthesis at Constant Temperature. , 157:339, July 1969. doi:10.1086/150072.

[3] S. I. Blinnikov, N. V. Dunina-Barkovskaya, and D. K. Nadyozhin. Equation of State of a Fermi Gas: Approximations for Various Degrees of Relativism and Degeneracy. , 106:171, Sept. 1996. doi:10.1086/192334.

[4] R. M. Cabezón, D. García-Senz, and E. Bravo. High-Temperature Combustion: Approaching Equilibrium Using Nuclear Networks. , 151(2):345–355, Apr. 2004. doi:10.1086/382352.

[5] R. M. Cabezón, D. García-Senz, and J. Figueira. SPHYNX: an accurate density-based SPH method for astrophysical applications. , 606:A78, Oct. 2017. arXiv:1607.01698, doi:10.1051/0004-6361/201630208.

[6] S. Chandrasekhar. The Maximum Mass of Ideal White Dwarfs. , 74:81, July 1931. doi:10.1086/143324.

[7] R. I. Epstein and W. D. Arnett. Neutronization and thermal disintegration of dense stellar matter. , 201:202–211, Oct. 1975. doi:10.1086/153875.

[8] C. J. Hansen. Some Weak Interaction Processes in Highly Evolved Stars. , 1(4):499–512, June 1968. doi:10.1007/BF00658771.

[9] A. M. Khokhlov. Delayed detonation model for type IA supernovae. , 245(1):114–128, May 1991.

[10] E. Mueller. Nuclear-reaction networks and stellar evolution codes - The coupling of composition changes and energy release in explosive nuclear burning. , 162(1-2):103–108, July 1986.

[11] K. Nomoto, F. K. Thielemann, and K. Yokoi. Accreting white dwarf models for type I supern. III. Carbon deflagration supernovae. , 286:644–658, Nov. 1984. doi:10.1086/162639.

[12] R. Pakmor, M. Kromer, F. K. Röpke, S. A. Sim, A. J. Ruiter, and W. Hillebrandt. Subluminous type Ia supernovae from the mergers of equal-mass white dwarfs with mass $\sim$0.9M$_{solar}$. , 463(7277):61–64, Jan. 2010. arXiv:0911.0926, doi:10.1038/nature08642.

[13] A. Parikh, J. José, I. R. Seitenzahl, and F. K. Röpke. The effects of variations in nuclear interactions on nucleosynthesis in thermonuclear supernovae. , 557:A3, Sept. 2013. arXiv:1306.6007, doi:10.1051/0004-6361/201321518.

[14] N. Prantzos, M. Arnould, and J. P. Arcoragi. Neutron Capture Nucleosynthesis during Core Helium Burning in Massive Stars. , 315:209, Apr. 1987. doi:10.1086/165125.

[15] F. K. Thielemann, K. Nomoto, and K. Yokoi. Explosive nucleosynthesis in carbon deflagration models of Type I supernovae. , 158(1-2):17–33, Apr. 1986.

[16] F. X. Timmes, R. D. Hoffman, and S. E. Woosley. An Inexpensive Nuclear Energy Generation Network for Stellar Hydrodynamics. , 129(1):377–398, July 2000. doi:10.1086/313407.

[17] S. E. Woosley and T. A. Weaver. Sub–Chandrasekhar Mass Models for Type IA Supernovae. , 423:371, Mar. 1994. doi:10.1086/173813.